



**HAL**  
open science

## **Acetylcholine production by type 2 innate lymphoid cells promotes mucosal immunity to helminth parasites**

Luke B Roberts, Corinna Schnoeller, Rita Berkachy, Matthew Darby, Jamie Pillaye, Menno J Oudhoff, Naveen Parmar, Claire Mackowiak, Delphine Sedda, Valérie Quesniaux, et al.

### ► To cite this version:

Luke B Roberts, Corinna Schnoeller, Rita Berkachy, Matthew Darby, Jamie Pillaye, et al.. Acetylcholine production by type 2 innate lymphoid cells promotes mucosal immunity to helminth parasites. *Science Immunology*, 2021, 6 (57), 10.1126/sciimmunol.abd0359 . hal-03429605

**HAL Id: hal-03429605**

**<https://hal.science/hal-03429605>**

Submitted on 15 Nov 2021

**HAL** is a multi-disciplinary open access archive for the deposit and dissemination of scientific research documents, whether they are published or not. The documents may come from teaching and research institutions in France or abroad, or from public or private research centers.

L'archive ouverte pluridisciplinaire **HAL**, est destinée au dépôt et à la diffusion de documents scientifiques de niveau recherche, publiés ou non, émanant des établissements d'enseignement et de recherche français ou étrangers, des laboratoires publics ou privés.

**Title**

Acetylcholine production by type 2 innate lymphoid cells promotes mucosal immunity to helminth parasites

**Authors**

Luke B. Roberts<sup>1,2</sup>, Corinna Schnoeller<sup>1</sup>, Rita Berkachy<sup>1</sup>, Matthew Darby<sup>3</sup>, Jamie Pillaye<sup>3,4</sup>, Menno J Oudhoff<sup>5</sup>, Naveen Parmar<sup>5</sup>, Claire Mackowiak<sup>3</sup>, Delphine Sedda<sup>6</sup>, Valerie Quesniaux<sup>6</sup>, Bernhard Ryffel<sup>6</sup>, Rachel Vaux<sup>1</sup>, Kleoniki Gounaris<sup>1</sup>, Sylvie Berrard<sup>7</sup>, David R. Withers<sup>4</sup>, William G. C. Horsnell<sup>3,4,6,\*</sup>, and Murray E. Selkirk<sup>1,8,\*</sup>

**Affiliations**

<sup>1</sup>Department of Life Sciences, Imperial College London, London, UK.

<sup>2</sup>School of Immunology and Microbial Sciences, King's College London, Great Maze Pond, London SE1 9RT, UK.

<sup>3</sup>Institute of Infectious Disease and Molecular Medicine, University of Cape Town, Cape Town, South Africa.

<sup>4</sup>College of Medical and Dental Sciences, University of Birmingham, Birmingham, UK

<sup>5</sup>CEMIR – Centre of Molecular Inflammation Research, Department of Clinical and Molecular Medicine, NTNU – Norwegian University of Science and Technology, 7491 Trondheim, Norway

<sup>6</sup>Laboratory of Molecular and Experimental Immunology and Neurogenetics, UMR 7355, CNRS-University of Orleans and Le Studium Institute for Advanced Studies, Rue Dupanloup, 45000 Orléans, France.

<sup>7</sup>Université de Paris, NeuroDiderot, Inserm, 75019 Paris, France

<sup>8</sup>Further information and requests for resources and reagents should be directed to and will be fulfilled by the Lead Contact, Murray E. Selkirk (m.selkirk@imperial.ac.uk)

\*Correspondence: ME Selkirk, [m.selkirk@imperial.ac.uk](mailto:m.selkirk@imperial.ac.uk); WGC Horsnell, [wghorsnell@gmail.com](mailto:wghorsnell@gmail.com)

31 **Abstract**

32  
33 Innate lymphoid cells (ILCs) are critical mediators of immunological and physiological responses at mucosal  
34 barrier sites. While neurotransmitters can stimulate ILCs, the synthesis of small-molecule neurotransmitters  
35 by these cells has only recently begun to be appreciated. Type 2 innate lymphoid cells (ILC2s) are shown  
36 here to synthesise and release acetylcholine (ACh) during parasitic nematode infection. The cholinergic  
37 phenotype of pulmonary ILC2s was associated with their activation state, could be induced by *in vivo*  
38 exposure to extracts of *Alternaria alternata* or the alarmin cytokines interleukin (IL)-33 and IL-25, and was  
39 augmented by IL-2 *in vitro*. Genetic disruption of ACh synthesis by murine ILC2s resulted in increased  
40 parasite burdens, impaired ILC2 proliferation, and reduced features of lung and gut barrier responses  
41 following *Nippostrongylus brasiliensis* infection. These data demonstrate a functional role for ILC2-derived  
42 ACh in expansion of ILC2s for maximal induction of type 2 immunity.

43

44 **One-sentence summary**

45 Synthesis of acetylcholine by type 2 innate lymphoid cells is important for optimal immune responses to  
46 helminth infection.

47

48 **MAIN TEXT**

49

50 **The manuscript should be a maximum of 15,000 words.**

51

52 **Introduction**

53

54 Although acetylcholine (ACh) is best known as a small-molecule neurotransmitter, cholinergic signalling  
55 also regulates the immune system. This is best described in the cholinergic anti-inflammatory pathway  
56 (CAIP), in which sensory perception of inflammatory stimuli leads to a vagal reflex culminating in  $\alpha 7$   
57 nicotinic receptor (nAChR) subunit-dependent inhibition of TNF- $\alpha$ , IL-1 $\beta$  and IL-18 production by splenic  
58 macrophages (1, 2). Definition of cells which synthesise ACh has been facilitated by the use of reporter  
59 mice to visualise expression of choline acetyltransferase (ChAT), the enzyme which synthesises ACh (3).  
60 CD4<sup>+</sup> T cells expressing an effector/memory (CD44<sup>+</sup>CD62L<sup>lo</sup>) phenotype were identified as the source of  
61 ACh in the spleen responsible for signalling to macrophages in the CAIP (4) and B cell-derived ACh  
62 inhibited neutrophil recruitment during sterile endotoxaemia (5). Additionally, CD4<sup>+</sup> and CD8<sup>+</sup> T cell

63 expression of ChAT induced by IL-21 is essential for tissue trafficking required for T cell-mediated control  
64 of viral infection (6). Adaptive immunity is also regulated by ACh, and optimal type 2 effector responses to  
65 the nematode parasite *Nippostrongylus brasiliensis* require signalling through the M3 muscarinic receptor  
66 (mAChR) (7).

67  
68 Group 2 innate lymphoid cells (ILC2s) play an important role in initiating type 2 immune responses,  
69 producing cytokines such as IL-13 and IL-5 which drive allergic inflammation and immunity to helminth  
70 infection (8, 9). ILC2s have recently been shown to be both positively and negatively regulated by  
71 neurotransmitters such as neuromedin U (NMU) (10–12) and noradrenaline (13), whereas group 3 innate  
72 lymphoid cells (ILC3s) upregulate lipid mediator synthesis in response to vagally-derived ACh (14).  
73 Interestingly, ILCs expressing receptors responsive to neurotransmitters co-localise with neurons in mucosal  
74 tissues, forming what have been termed neuroimmune cell units (NICUs) (15). Additionally ILC2s express  
75 the neuropeptide calcitonin gene-related protein, CGRP (16). Recently, expression of tryptophan  
76 hydroxylase 1 (Tph1) – the rate-limiting enzyme for the synthesis of the small-molecule neurotransmitter  
77 serotonin, as well as production of serotonin itself by ILC2s has been described (17).

78  
79 In this study we demonstrate that pulmonary ILC2s upregulate their capacity to synthesise and release ACh  
80 during infection with *N. brasiliensis* and show that the cholinergic phenotype of ILC2s is induced by the  
81 alarmin cytokines IL-33 and IL-25. Disruption of the ability of ILC2s to synthesise ACh by generation of  
82 *Rora*<sup>Cre+</sup>*Chat*<sup>LoxP</sup> transgenic mice resulted in impaired immunity to *N. brasiliensis*, accompanied by reduced  
83 total expression of type 2 cytokines IL-5 and IL-13 and the mucins Muc5b and Muc5ac in the lung, in  
84 addition to altered intestinal barrier responses. These data demonstrate that production and release of ACh  
85 by ILC2s is an important factor in driving type 2 immunity.

**Results****ILC2s synthesise and release acetylcholine during type 2 immunity**

The cholinergic phenotype of immune cells was monitored across the time course of a primary infection with *N. brasiliensis* using ChAT-eGFP<sup>BAC</sup> mice (3). From day 4 post infection (D4 p.i., immediately following the pulmonary migratory phase of parasite larvae) until at least D21 p.i., (long past the peak of the acute phase of infection-driven inflammation) the proportion and number of CD45<sup>+</sup> cells in lung tissue which expressed ChAT (ChAT-eGFP<sup>+</sup>) was increased compared to uninfected (naïve) controls (**Figure 1A**). Analysis of ChAT-eGFP<sup>+</sup> leucocytes revealed that most of these cells were from lymphoid rather than myeloid lineages, as previously reported in other models and tissues (5) (**Figure 1B**). Of the populations screened, only ILC2s significantly upregulated the proportion of cells expressing ChAT-eGFP at an early time point (D4) in infection (**Figure 1B**).

As a cholinergic phenotype for ILC2s had not been previously described, we explored this further. Kinetic analysis of ChAT-eGFP expression by ILC2s in lung and bronchoalveolar lavage (BAL) samples during infection showed a significant increase by D4 p.i., peaking at D7, and remained elevated in both sites at D21. The proportion of ILC2s which were ChAT-eGFP<sup>+</sup> was consistently much greater in BAL than in the lungs (**Figure 1C, 1D**). Real-time RT-qPCR confirmed that *Chat* expression in pulmonary ChAT-eGFP<sup>+</sup> ILC2s from infected ChAT-eGFP<sup>BAC</sup> mice was upregulated in comparison to ILC2 from uninfected ChAT-eGFP<sup>BAC</sup> animals, as well as to ChAT-eGFP<sup>neg</sup> ILC2, validating our reporter system (**Figure 1E**). HPLC-mass spectrometry was used to verify that WT ILC2s synthesise and release ACh and showed that this was greatly enhanced during parasite infection (**Figure 1F**). In these experiments, cells were isolated from infected animals at D11 p.i. to maximise the number of ACh-producing ILC2s obtained. Additionally we observed that ChAT-eGFP<sup>+</sup> ILC2s had a significantly increased mean fluorescence intensity (MFI) for the IL-33 receptor subunit ST2 compared to ChAT-eGFP<sup>-</sup> cells at D4 and D7 p.i. (**Figure 1G**) and also for

111 inducible T cell co-stimulator (ICOS) at D7 p.i. (**Figure 1H**), suggesting that ChAT expression is associated  
112 with ILC2 activation state.

113  
114 A significant degree of heterogeneity exists amongst ILC2s, with subtypes such as tissue-resident ‘natural’  
115 ILC2s (nILC2s) and tissue-infiltrating ‘inflammatory’ ILC2s (iILC2s) previously described and delineated  
116 on the basis of differential levels of phenotypic marker expression in the lung (18). Furthermore, the  
117 functions of these subtypes have physiological relevance with regards to anti-helminth immune responses  
118 such as pulmonary mucus production (9). To further characterise pulmonary ChAT-eGFP<sup>+</sup> ILC2s and probe  
119 whether these cells belonged to a defined subtype of ILC2s, we infected ChAT-eGFP<sup>BAC</sup> mice with *N.*  
120 *brasiliensis* and analysed pulmonary ILC2s at D7 p.i, utilising an extended panel of phenotypic markers  
121 (**Figure 2A**). To assess whether ChAT-eGFP<sup>+</sup> ILC2s represented previously recognised nILC2 and iILC2  
122 subsets, we used t-distributed stochastic neighbor embedding (t-SNE) analysis (omitting ChAT-eGFP  
123 expression as a component for clustering), to first identify populations of ILC2s (CD45<sup>+</sup>Lineage-  
124 CD127<sup>+</sup>ICOS<sup>+</sup> CD90<sup>+</sup> cells expressing either or both ST2 and IL-17RB) which most represented  
125 conventional nILC2 (IL-17RB<sup>-</sup>ST2<sup>+</sup>CD90<sup>+</sup>Klrg1<sup>lo/-</sup>) and iILC2 (IL-17RB<sup>+</sup>ST2<sup>lo/-</sup> CD90<sup>lo</sup> Klrg1<sup>hi</sup>) subsets  
126 (**Figure 2A**). We also identified additional clusters which we designated ‘nILCa’ and ‘iILC2a’ on the basis  
127 that these populations appeared to represent nILC2-like and iILC2-like cells in a higher state of cellular  
128 activation, given their differential expression of IL-17RB, but dual expression of ST2 and Klrg1, and higher  
129 expression of CD90. Given our previous observation that ChAT-eGFP expression in ILC2s appeared to  
130 correlate with cellular activation, we reasoned that these groupings may be relevant for comparative analysis.  
131 Indeed, it appeared that the majority of ILC2s expressing high levels of ChAT-eGFP were located amongst  
132 these activated nILC2a and iILC2a populations (**Figure 2B**). Analysis was again carried out utilising t-SNE  
133 (with ChAT-eGFP expression incorporated into clustering), and ChAT-eGFP<sup>+</sup> clusters could be segregated  
134 into 3 distinct populations, designated C1-C3 (**Figure 2C**). Based on a combination of marker expression  
135 and comparative assessment of the ChAT-eGFP<sup>+</sup> clusters against the 4 pre-defined reference subtypes,  
136 population C1 appeared most similar to conventional nILC2 cells, whilst C2 shared the phenotypic profile  
137 of nILC2a, and C3 was most similar to iILC2a (**Figure 2D**). The greatest proportion of ChAT-eGFP<sup>+</sup> ILC2s  
138 were represented by population C2, followed by C3, then C1 (**Figure 2E**). A similar analysis of marker

139 expression of the very few ChAT-eGFP<sup>+</sup> cells in naïve ChAT-eGFP<sup>BAC</sup> lungs revealed that these cells clearly  
140 showed a nILC2-like profile, with no obvious differences in marker expression to that of total ChAT<sup>neg</sup>  
141 ILC2s, including ICOS and ST2 (**Figure 2F, 2G, 2H**). A different scenario was observed in infected mice  
142 however, with a disparate profile for total ChAT-eGFP<sup>+</sup> ILC2s relative to total ChAT<sup>neg</sup> ILC2s (**Figure 2F,**  
143 **2G, 2H**), corroborating the findings of previous analyses (**Figure 1G, 1H**). ChAT-eGFP<sup>+</sup> ILC2s therefore  
144 do not appear to represent a singular ILC2 subtype during *N. brasiliensis* infection. One interpretation of  
145 these data may be that in infected, population C1 represents the ChAT-eGFP<sup>+</sup> nILC2-like cells found in  
146 naïve mice, while populations C2 and C3 represent nILC2-like and iILC2-like populations induced to  
147 express ChAT as a result of infection, supporting our hypothesis that ChAT-eGFP expression in ILC2s is  
148 predominantly associated with cellular activation.

149  
150 To investigate whether ChAT-eGFP expression by ILC2s was solely a feature of pulmonary tissues, we  
151 examined ILC2s from mesenteric lymph nodes (MLNs) ChAT-eGFP<sup>+</sup> ILC2 were found in MLNs of both  
152 naïve and *N. brasiliensis*-infected mice (**Figure 3A**). However, as in pulmonary populations, the proportion  
153 of ILC2s expressing ChAT-eGFP increased as a result of infection (**Figure 3B**), as did the total numbers  
154 (**Figure 3C**). Interestingly, ChAT-eGFP<sup>+</sup> ILC2s in the MLNs of infected mice displayed a different  
155 phenotypic profile to ChAT-eGFP<sup>neg</sup> ILC2s, particularly evident when observing Klrp1 expression, which  
156 was restricted to ChAT-eGFP<sup>+</sup> cells, accompanied by higher expression of ST2, ICOS, and (generally) IL-  
157 17R (**Figure 3D, 3E, 3F**). This difference in marker expression was also apparent between ChAT-eGFP<sup>+</sup>  
158 and ChAT-eGFP<sup>neg</sup> ILC2s of naïve MLNs, although expression levels were much greater following  
159 infection, as expected (**Figure 3E, 3F**). Given the difficulty in isolating viable leucocytes from the small  
160 intestinal lamina propria (siLP) of *N. brasiliensis* infected mice, we were not able to analyse ChAT-eGFP  
161 expression by flow cytometry from siLP ILC2 during infection. However, siLP ILC2s from naïve mice did  
162 not greatly express ChAT-eGFP (**Figure 3G**), indicating that siLP ILC2s do not constitutively display a  
163 cholinergic phenotype in the absence of infection, akin to our observations in naïve lungs. Overall, these  
164 data indicate that ChAT-eGFP expression by ILC2s is not limited to pulmonary populations, and further  
165 support association of the cholinergic phenotype with cellular activation.

167 Next, we tested if induction of the cholinergic phenotype in ILC2s was specific to parasite infection or a  
168 general feature of type 2 immunity. Mice exposed to extracts of *Alternaria alternata*, a fungal plant pathogen  
169 linked to exacerbation of asthma, develop rapid onset type 2-driven eosinophilic airway inflammation(19).  
170 ChAT-eGFP<sup>BAC</sup> and WT mice were dosed intranasally with *Alternaria* extract or phosphate buffered saline  
171 (PBS), culled 24 hours later and lung cells analysed for ChAT-eGFP expression. Successful induction of a  
172 type 2 response was confirmed by pulmonary eosinophilia (**Figure S1A**). Challenge with *Alternaria* induced  
173 small but significant increases in ChAT-eGFP expression in some lymphocyte populations, including CD4<sup>+</sup>  
174 T cells and NKT cells, although expression in granulocytes was again unaffected (**Figure S1B**). However,  
175 as in nematode infection, the greatest proportional increase in ChAT-eGFP expression was observed in  
176 ILC2s (**Figures S1C, S1D**).

177  
178 These data show that ILC2s have an inducible cholinergic phenotype, and that this is activated in response  
179 to parasitic nematode infection and exposure to a fungal allergen. This identifies ILC2s as the principle  
180 innate source of ACh during type 2 immune responses.

### 182 **IL-25 and IL-33 induce the cholinergic phenotype of pulmonary ILC2s**

183 As our data suggested that ChAT expression was associated with cellular activation, we investigated whether  
184 known activators of ILC2s could induce this phenotype. Ex vivo stimulation of CD45<sup>+</sup> cells isolated from  
185 naïve ChAT<sup>BAC</sup>-eGFP reporter mice with IL-33, but not IL-7 enhanced ILC2 ChAT-eGFP expression,  
186 suggesting that activation through alarmin signalling pathways specifically drives the ILC2 cholinergic  
187 phenotype (**Figure 4A**). To explore this further, we dosed reporter mice intranasally with IL-33, IL-25 and  
188 thymic stromal lymphopietin (TSLP), and analysed ChAT-eGFP expression on pulmonary ILC2s 24 hrs  
189 later. IL-25 and IL-33 both induced ChAT-eGFP expression on ILC2s, with IL-25 having the greatest effect;  
190 no effect was observed with TSLP (**Figure 4B-C**). Analysis of other leukocyte populations in the lung  
191 showed that activation of ChAT-eGFP expression by alarmins was only observed in ILC2s at the time point  
192 investigated (**Figure 4D**).

195 The observation that IL-25 appeared to promote greater upregulation of ChAT expression than IL-33, 24  
196 hours after administration of recombinant cytokines, was interesting. Lung ILC2s predominantly express the  
197 IL-33 receptor in naïve animals at immunological baseline, while iILC2s expressing the IL-25 receptor are  
198 thought to migrate to the lung from sites such as the gut following tissue damage such as that caused by  
199 helminth infection (18). It is possible that administration of recombinant IL-25 mobilised ILC2s from outside  
200 the lungs to migrate to the pulmonary tract and that these cells contributed to the increase in ChAT-eGFP<sup>+</sup>  
201 ILC2s, although this is unlikely as it would have to happen within 24 hours. However, it is noteworthy that  
202 although the proportion of IL-17RB-expressing ILC2s in the lungs increases significantly following *N.*  
203 *brasiliensis* infection (Figure 4E, 4F), around a fifth of ILC2s from the lungs of naïve mice (those found in  
204 naïve ChAT-eGFP<sup>BAC</sup> mice used in our study) expressed IL-17RB as well as ST2 (Figure 4E, 4F), and thus  
205 have the capacity to respond to administration of exogenous IL-25.

206  
207 To assess the capacity of lung-resident ILC2s to upregulate ChAT-eGFP in response to exogenous alarmin  
208 cytokine treatment, we isolated CD45<sup>+</sup> cells from the lungs of naïve ChAT<sup>BAC</sup>-eGFP reporter mice by FACS  
209 and stimulated them *in vitro* with combinations of recombinant cytokines and assayed ChAT-eGFP  
210 expression by ILC2s 24 hrs later. IL-2 is also known to promote proliferation and cytokine production by  
211 ILC2s (20, 21) and so we also examined the capacity for IL-2 to upregulate ChAT-eGFP by the cells.  
212 Stimulation with IL-25 and IL-33 both enhanced ChAT-eGFP expression. However, IL-2 also induced  
213 ChAT-eGFP expression by ILC2s and moreover, an additive effect of stimulation with IL-2 and either IL-  
214 33 or IL-25 was observed (Figure 4G-H).

### 216 **RoR $\alpha$ -driven disruption of ChAT expression impairs pulmonary type 2 immunity to *N. brasiliensis***

217 To determine whether synthesis of ACh by ILC2s played a role in immunity to helminth infection, we  
218 generated *Rora*<sup>Cre+</sup>*Chat*<sup>LoxP</sup> mice in which a portion of the coding domain of the *Chat* gene is floxed (22) and  
219 excised by Cre-recombinase expressed under the control of *Rora* regulatory elements (23) (Figure S2A-B).  
220 The use of *Rora*<sup>Cre+</sup> mice to selectively carry out gene deletion in ILC2s has been previously demonstrated  
221 (24). Successful *Chat* deletion in *Rora*<sup>Cre+</sup>*Chat*<sup>LoxP</sup> ILC2s was confirmed by PCR analysis and sequencing  
222 (Figure S2C, S2D, S2E). Infection of *Rora*<sup>Cre+</sup>*Chat*<sup>LoxP</sup> and *Chat*<sup>LoxP</sup> littermate controls with *N. brasiliensis*

223 revealed that although numbers of larvae recovered from the lungs were not significantly different between  
224 genotypes at day 2 post infection (p.i.), significantly higher intestinal worm burdens were observed at day 6  
225 p.i. in *Rora*<sup>Cre+</sup>*Chat*<sup>LoxP</sup> mice, indicating delayed parasite clearance in the absence of ILC2 ChAT expression  
226 (**Figure 5A**). Interestingly, *Rora*<sup>Cre+</sup>*Chat*<sup>LoxP</sup> mice had reduced pulmonary eosinophilia compared to controls  
227 following *N. brasiliensis* infection, indicative of a suppressed type 2 immune response (**Figure 5B**).  
228 Significantly reduced expression of *Il5* and *Il13* in total lung tissue of infected *Rora*<sup>Cre+</sup>*Chat*<sup>LoxP</sup> samples,  
229 relative to controls supported this observation (**Figure 5C**). A primary role for IL-13 during the anti-helminth  
230 immune response is to drive goblet cell hyperplasia and mucin production at epithelial barrier sites including  
231 the lung, where the predominant gel-forming mucins secreted by goblet cells are *Muc5b* and *Muc5ac* (25).  
232 Accordingly, infected *Rora*<sup>Cre+</sup>*Chat*<sup>LoxP</sup> at D6 p.i. demonstrated significantly reduced expression of *Muc5b*  
233 and *Muc5ac* in total lung tissue (**Figure 5D**). PAS staining also revealed significantly reduced airway mucins  
234 in *Rora*<sup>Cre+</sup>*Chat*<sup>LoxP</sup> lungs compared to the robust response observed in *Chat*<sup>LoxP</sup> airways (**Figure 5E-F**).

### 236 **Impaired immunity to *N. brasiliensis* in *Rora*<sup>Cre+</sup>*Chat*<sup>LoxP</sup> mice is associated with defective intestinal** 237 **barrier responses**

238 To assess whether a defective response to *N. brasiliensis* infection following RoR $\alpha$ -mediated ChAT  
239 disruption was confined to pulmonary ILC2s and associated responses in the lung, we also assessed  
240 responses in the small intestine. Intestinal epithelial effector responses characteristic of type 2 immunity  
241 include goblet and tuft cell hyperplasia. In the small intestine, we observed a decrease in periodic acid-Schiff  
242 (PAS)-positive goblet cells comparing *Rora*<sup>Cre+</sup>*Chat*<sup>LoxP</sup> samples to *Chat*<sup>LoxP</sup> controls (**Figure 6A, 6B**).  
243 Furthermore, we quantified tuft cells as analysed through immunofluorescent staining of doublecortin-like  
244 kinase 1 (*Dclk1*) (**Figure 6C**). We found that, although *Rora*<sup>Cre+</sup>*Chat*<sup>LoxP</sup> mice did not have a statistically  
245 reduced number of tuft cells overall (**Figure 6D**), the ratio of cells present in villus to crypt regions was  
246 significantly lower in *Rora*<sup>Cre+</sup>*Chat*<sup>LoxP</sup> mice (**Figure 6E**). In line with delayed worm expulsion (**Figure**  
247 **5A**), these data reflect an inhibited onset of type 2 immunity in these animals.

### 249 **ILC2-derived ACh promotes autocrine population expansion of ILC2s to facilitate optimal anti-** 250 **helminth type 2 immunity.**

251 ILC2s are the major innate source of IL-13 during helminth infection and ILC2-derived IL-13 is critical for  
252 expulsion of *N. brasiliensis* and induction of mucin expression in response to helminth infections (8, 9, 26).  
253 Given our finding that RoR $\alpha$ -mediated disruption of *Chat* expression negatively impacted the type 2 immune  
254 response to *N. brasiliensis* infection, we next analyzed whether ILC2s themselves were affected by removing  
255 their capacity to synthesise ACh. Although total number of ILC2s in the lungs increased following *N.*  
256 *brasiliensis* infection regardless of genotype, significantly fewer ILC2s were found in *Rora*<sup>Cre+</sup>*Chat*<sup>LoxP</sup> lungs  
257 (Figure 7A). Of note, slightly fewer ILC2s were also observed in *Rora*<sup>Cre+</sup>*Chat*<sup>LoxP</sup> lungs compared to  
258 *Chat*<sup>LoxP</sup> lungs at baseline (Figure 7A) and the fold change for infection-induced increase in ILC2 numbers  
259 at this timepoint was not significantly different between genotypes (Figure S3A), possibly indicative of a  
260 homeostatic requirement for *Chat* by ILC2s. A similar finding was made in the MLNs of infected  
261 *Rora*<sup>Cre+</sup>*Chat*<sup>LoxP</sup> mice, where significantly fewer ILC2s were observed in comparison to infected controls  
262 (Figure S3B). Although ILC2s from *Rora*<sup>Cre+</sup>*Chat*<sup>LoxP</sup> mice could still express IL-5 and IL-13 (Figure S3C-  
263 S3G) and upregulated cytokine expression in response to infection on a similar per-cell basis to *Chat*<sup>LoxP</sup>  
264 ILC2s (Figure S3E, S3G), the overall number of IL-13 and IL-5 expressing ILC2s was significantly reduced  
265 in infected *Rora*<sup>Cre+</sup>*Chat*<sup>LoxP</sup> lungs at day 6 p.i. (Figure 7B).

266  
267 Ki67 staining of ILC2s revealed that *Rora*<sup>Cre+</sup>*Chat*<sup>LoxP</sup> ILC2s were less proliferative than *Chat*<sup>LoxP</sup> ILC2s  
268 following infection (Figure 7C, 7D), resulting in a significantly smaller pool of proliferative ILC2s overall  
269 (Figure 7E). Additionally, expression of ICOS was significantly reduced on *Rora*<sup>Cre+</sup>*Chat*<sup>LoxP</sup> ILC2s  
270 following infection, indicative of a decreased ILC2 activation state (Figure 7F, 7G). Similar observations  
271 were made for activation markers ST2 and ICOS on ILC2s in the MLNs of infected *Rora*<sup>Cre+</sup>*Chat*<sup>LoxP</sup> (Figure  
272 S3H, S3I), indicating that the effects caused by prevention of ACh synthesis were not confined to pulmonary  
273 ILC2s. We also analysed the number of CD4<sup>+</sup> lung T cells (Figure S4A), their proliferative capacity (Figure  
274 S4B, S4C), and expression of IL-13 (Figure S4D), but found that these parameters were unaffected by  
275 genotype, indicative of an ILC2-specific effect of *Chat* deletion in *Rora*<sup>Cre+</sup>*Chat*<sup>LoxP</sup> mice.

276  
277 Lymphocytes are known to express acetylcholine receptors (AChRs), although the full complement of  
278 muscarinic (mAChR) and nicotinic (nAChR) receptors expressed by ILC2s has not been defined to our

279 knowledge (7, 27). Using cDNA prepared from FACS-purified ChAT-eGFP<sup>+</sup> and ChAT-eGFP<sup>neg</sup> lung  
280 ILC2s from *N. brasiliensis*-infected ChAT-eGFP<sup>BAC</sup> mice, we observed expression of transcripts for multiple  
281 mAChRs in addition to the  $\alpha 7$ nAChR (27). Interestingly, there appeared to be a degree of differential  
282 expression between ChAT-eGFP<sup>+</sup> and ChAT-eGFP<sup>neg</sup> with regards to AChR subtypes (Figure 7H, 7I). In  
283 order to determine whether ACh might act as an autocrine factor to influence proliferation and activation of  
284 the cells, we isolated WT ILC2s from the lungs of *N. brasiliensis*-infected C57BL/6J mice and cultured them  
285 in vitro with IL-7 and IL-2 alone or in the presence of the mAChR antagonist 1,1-dimethyl-4-  
286 diphenylacetoxypiperidinium iodide (4-DAMP) or the nAChR antagonist mecamylamine. Addition of 4-  
287 DAMP significantly restricted the proliferative capacity of the cells, while mecamylamine had no effect  
288 when compared with vehicle-treated control cultures (Figure 7J, 7K, 7L). These data suggest that  
289 activation-induced ACh synthesis by ILC2s plays a role in mAChR-mediated autocrine promotion of ILC2  
290 proliferation and population expansion.

291  
292 In summary these data support the hypothesis that ILC2-derived ACh plays a critical role in mounting robust  
293 type 2 immunity and control of *N. brasiliensis* infection.

## 295 Discussion

296 ILC2s play a pivotal role in translating epithelial cell cytokine production into robust type 2 immune  
297 responses. Here we show that in addition to the cytokines IL-13 and IL-5, production of ACh by ILC2s is a  
298 requirement for optimal type 2-driven immunity to *N. brasiliensis*. The alarmin cytokines IL-25 and IL-33  
299 were demonstrated to upregulate ChAT-eGFP expression by ILC2s both in vivo and in vitro. As expression  
300 of ChAT by B cells is induced by MyD88-dependent Toll-like receptor signalling (5), we hypothesised that  
301 IL-33 might regulate the ILC2 cholinergic phenotype, as members of the IL-1 family such as IL-33 also  
302 signal through this adapter protein. However, IL-25 was also a major regulator of ChAT expression,  
303 demonstrating that MyD88-dependent signalling is not essential for this in ILC2s. A factor common to both  
304 signalling pathways, such as the signal transducer TRAF6, may be required for inducible ChAT expression  
305 in ILC2s. TSLP, which does not signal through either MyD88 or TRAF6-dependent pathways, did not  
306 induce ChAT expression in ILC2s when administered in vivo at the same dose. However, although TSLP

307 has been reported to influence cutaneous ILC2 activation (28), most studies identify IL-25 and IL-33 as the  
308 major inducers of ILC2 responses in the lung and gut (26, 29).

309  
310 IL-2 was also shown to induce ChAT expression, both by itself or in combination with IL-25 and IL-33. IL-  
311 2 is a critical regulator of ILC2s, driving cell survival and proliferation, and augmenting type 2 cytokine  
312 production (30). Thus, the cholinergic phenotype of ILC2s is clearly induced by a number of stimuli which  
313 activate these cells. Recently, neuropeptides such as NMU, vasoactive intestinal peptide (VIP) and CGRP  
314 and the small molecule neurotransmitter serotonin have also been shown to regulate ILC2 activation and  
315 effector activity (10–12, 16, 17, 31). If these molecules can also induce or modulate ChAT expression in  
316 ILC2s, this raises the possibility of bi-directional neuroimmune communication involving ILC2s and ACh-  
317 responsive neurons within NICUs.

318  
319 Impairment of ACh synthesis by ILC2s resulted in a lower number of cells, a deficit in ILC2-derived effector  
320 cytokine production and significant restriction of anti-helminth type 2 responses in the lungs and small  
321 intestine, tissue sites physiologically relevant to the parasite's life cycle. One interpretation of this may be  
322 that ILC2-derived ACh acts as an autocrine signal to aid population expansion. One way this could  
323 hypothetically occur is if ACh acts to promote expression of autocrine survival factors such as IL-9 (32), the  
324 expression of which has been shown to be promoted by neuropeptide signaling in ILC2s (33). The labile  
325 nature of ACh, due to high levels of circulating butyrylcholinesterase in tissue fluids (34) makes it likely  
326 that ILC2-derived ACh will function over relatively short distances, as would be the case during autocrine  
327 signaling. In support of this, we demonstrated that ILC2s express a range of nicotinic and muscarinic ACh  
328 receptors, and expression of the  $\alpha 7$  nAChR by ILC2s has also been previously described (27). In vitro culture  
329 of ILC2s with 4-DAMP led to a reduction in ILC2 proliferative capacity. Thus it is plausible that autocrine  
330 cholinergic signalling in ILC2s operates through mAChRs in order to promote their own expansion.  
331 Although 4-DAMP is frequently quoted as M3/M1-selective, studies on rat and human receptors show that  
332 it has potent effects on M1, M3, M4 and M5 receptors ( $K_i$  less than 1 nM), and also good activity against  
333 M2 ( $K_i$  4-7 nM). (35, 36). Thus, at the concentration used in our experiments, 4-DAMP would be expected  
334 to antagonise all mAChR subtypes.

335

336 Anticholinergics in the form of mAChR antagonists such as tiotropium are widely used to treat asthma and  
337 chronic obstructive pulmonary disease (37). These antagonists alleviate bronchoconstriction and mucus  
338 production, and are well documented to ameliorate allergen-induced airway inflammation and remodelling  
339 (38, 39), which may be accompanied by reduced type 2 cytokine production (40). In contrast, a recent report  
340 indicated that an  $\alpha 7$ -selective nAChR agonist reduced ILC2 effector function and airway hyperreactivity in  
341 an *Alternaria* allergic inflammation model (27). It is thus likely that signalling through different AChRs on  
342 ILC2s can result in disparate outcomes, and this could be affected by altered receptor expression under  
343 differing physiological conditions.

344

345 A surprising observation was that ChAT expression by ILC2s was maintained long after helminth  
346 eradication from the host (D21 p.i.). In addition to critical type 2 effector functions, ILC2s play important  
347 direct and indirect roles in promotion of wound healing and tissue repair (41, 42). It will be interesting to  
348 determine whether ACh production by ILC2s plays a role during later, pro-repair activities in addition to the  
349 acute inflammatory phase of infection.

350

351 A limitation of our study is that, despite the critical role of RoR $\alpha$  in ILC2 development (43, 44), expression  
352 of RoR $\alpha$  is not confined to ILC2s (45). Therefore, despite the fact that the *Rora*<sup>Cre+</sup> mouse has previously  
353 been used to successfully facilitate gene deletion in ILC2s in vivo (24), it is feasible that deletion in other  
354 cell types may also have occurred, and that this may have contributed to our observations. However,  
355 proliferation and Th<sub>2</sub> cytokine production by CD4<sup>+</sup> T cells, which are also known to express this transcription  
356 factor, were not affected during *N. brasiliensis* infection of *Rora*<sup>Cre+</sup>*Chat*<sup>LoxP</sup> mice.

357

358 Helminths have evolved sophisticated strategies to promote survival in their hosts, targeted at key drivers of  
359 anti-parasite immunity (46). Secretion of acetylcholinesterases (AChEs) by parasitic nematodes has been  
360 postulated to promote parasite persistence via inhibition of cholinergic signalling in relation to the 'weep and  
361 sweep' response, characterised by intestinal smooth muscle contraction and fluid secretion from epithelial  
362 cells (47). Our current study demonstrates that production of ACh by ILC2s is a key factor in population

363 expansion, driving maximal type 2 immunity and mucin expression, suggesting that hydrolysis of ACh by  
364 secreted AChEs may also act to suppress this to a level which allows parasite establishment within the host.

## 366 **Materials and Methods**

369 **Animals and parasite infection.** This study was approved by the Animal Welfare Ethical Review Board at  
371 Imperial College London and was licensed by and performed under the UK Home Office Animals (Scientific  
372 Procedures) Act Personal Project Licence number 70/8193: 'Immunomodulation by helminth parasites'.  
373 C57BL/6J mice, aged 6-8 weeks old were purchased from Charles River. ChAT-eGFP<sup>BAC</sup> (3) were purchased  
374 from Jackson Laboratories and subsequently bred in-house. *Chat*<sup>Loxp</sup> mice were generated as previously  
375 described (22) and were backcrossed to F6-F10 generations on a B6 background with *Rora*<sup>Cre+</sup> (23) a kind gift  
376 from Andreas Zembrzycki (Salk Institute, La Jolla, CA) to generate the *Rora*<sup>Cre+</sup>*Chat*<sup>Loxp</sup> mice used in this  
377 study. Mice were infected with *N. brasiliensis* by sub-cutaneous (s.c.) inoculation with 500 infective larvae  
378 and parasites maintained by established methods (48).

380 **Murine model of allergic airway inflammation.** Extracts of *Alternaria alternata* were obtained as a gift  
381 from Henry McSorley (University of Edinburgh) or purchased as lyophilised protein extract from Greer  
382 Laboratories (USA). Mice were lightly dosed with isoflurane before intranasal administration with 50 µg *A.*  
383 *alternata* extract in a final volume of 50 µl PBS. Mice were exposed to a single dose of *A. alternata* for 24  
384 hours. Control animals were dosed with 50 µl PBS in the same schedule.

386 **Cytokines.** Recombinant murine cytokines were purchased from R&D (IL-25, TSLP) or Peprotech (IL-33,  
387 IL-2, IL-7) and used at 50 ng ml<sup>-1</sup> *in vitro* or administered in 50 µl doses at 10 µg ml<sup>-1</sup> *in vivo* as indicated.

389 **Tissue preparation.** For isolation of bronchoalveolar cells, lungs were lavaged twice in a total of 2 ml PBS  
390 with 0.2% BSA and 2 mM EDTA. Erythrocytes were lysed, leukocytes resuspended and counted. For lung  
391 single cell suspensions, lungs were perfused via cardiac puncture with 10 ml PBS then infused with 1.5 ml  
392 PBS containing 5 mg ml<sup>-1</sup> dispase II neutral protease (Sigma) via the trachea. The thymus and lung-draining

393 lymph nodes were removed, lungs ligatured, removed into 1.5 ml digest solution, incubated at room  
394 temperature for 25 min, then for a further 30 min at 37°C. Lungs were mechanically dissociated in Dulbecco's  
395 Minimal Essential Medium (DMEM) with 25 mM HEPES and 100 U ml<sup>-1</sup> DNase I (Sigma), and incubated  
396 at room temperature for 10 min. Samples were passed through 100 µm cell strainers and erythrocytes lysed.

397 Single cell preparations of mesenteric lymph nodes were generated by mechanical dissociation through a 40  
398 µm cell strainer followed by standard erythrocyte lysis. Small intestinal lamina propria (siLP) leucocytes  
399 were isolated with EDTA-based stripping of the intestinal epithelial layer followed by tissue digestion using  
400 collagenase-D (0.5 mg ml<sup>-1</sup>), Dispase-II (1.5 mg ml<sup>-1</sup>) and 10 µg ml<sup>-1</sup> DNase I in HBSS without Mg<sup>2+</sup> or  
401 Ca<sup>2+</sup> + 2% FCS. A 40-80% Percoll gradient separation was used to isolate a leucocyte enriched siLP sample.  
402  
403

404 **Flow cytometry and cell sorting.** Single cell suspensions were stained with fixable viability dyes  
405 (Invitrogen), then treated with rat anti-mouse CD32/CD16 (FcBlock, BD Biosciences), washed, then stained  
406 for extracellular markers using fluorophore conjugated monoclonal antibodies (eBioscience, Miltenyi Biotec  
407 or Biolegend). For intracellular staining, cells were fixed for 30 min at room temperature, then permeabilised  
408 using the FoxP3/transcription factor staining buffer kit (eBioscience) and stained with fluorochrome-  
409 conjugated antibodies. Unstained samples and fluorescence minus one controls were used as appropriate.  
410 When analyzing eGFP fluorescence from ChAT-eGFP<sup>BAC</sup> reporter mouse cells, WT (C57BL/6J) cells were  
411 used as negative controls to set eGFP gates. Samples were analysed on a BD LSR Fortessa™ analyser. For  
412 FACS sorting of ILC2s, lung tissue was processed to a single cell suspension as described, the lineage  
413 negative population enriched by magnetic activated cell sorting, depleting other cells via a PE-conjugated  
414 lineage cocktail (Miltenyi Biotec), then ILC2s sorted on a BD FACS ARIA III cell sorter.  
415

416 **Immunophenotyping of leucocyte populations.** Unless otherwise stated, leucocyte populations were  
417 identified by flow cytometry by gating live cells, followed by single cell and CD45<sup>+</sup> gating, and then using  
418 the following markers: ILC2; lineage<sup>-</sup>CD90<sup>+</sup>ICOS<sup>+</sup>ST2<sup>+</sup>CD127<sup>+</sup>. T cells; CD19<sup>-</sup>CD3ε<sup>+</sup>. CD4<sup>+</sup> T cells; CD19<sup>-</sup>  
419 CD3ε<sup>+</sup>DX5<sup>-</sup>CD4<sup>+</sup>CD8α<sup>-</sup>. CD8<sup>+</sup> T cells; CD19<sup>-</sup>CD3ε<sup>+</sup>DX5<sup>-</sup>CD4<sup>+</sup>CD8α<sup>+</sup>. B cells; CD19<sup>+</sup>CD3ε<sup>-</sup>B220<sup>+</sup>. γδ T  
420 cells; CD19<sup>-</sup>CD3ε<sup>+</sup>DX5<sup>-</sup>CD4<sup>-</sup>CD8α<sup>+</sup>GL3<sup>+</sup>. NK-T cells (NKT); CD19<sup>-</sup>CD3ε<sup>+</sup>DX5<sup>+</sup>. Natural Killer cells

421 (NK); CD19<sup>-</sup>CD3 $\epsilon$ <sup>-</sup>DX5<sup>+</sup>Fc $\epsilon$ R1<sup>-</sup>. Neutrophils; CD11b<sup>+</sup>SIGLEC-F<sup>-</sup>GR-1<sup>hi</sup>CD11c<sup>lo</sup> Eosinophils;  
422 CD11b<sup>+</sup>SIGLEC-F<sup>+</sup>GR-1<sup>lo</sup>CD11c<sup>lo</sup>. Basophils; CD19<sup>-</sup>CD3 $\epsilon$ <sup>-</sup>DX5<sup>+</sup>Fc $\epsilon$ R1<sup>+</sup>. The lineage panel consisted of  
423 antibodies to CD3, CD4, CD8, B220, CD19, TER119, CD49b, Fc $\epsilon$ RI and CD11b. Additional markers  
424 analysed for phenotyping and functional analysis were assessed using antibodies against Klrp1, IL-17RB,  
425 IL-5 and IL-13.

426

427 **Ki67 and intracellular cytokine staining.** To assess proliferative capacity of cells directly ex vivo, samples  
428 were processed to single cell suspension as described and rested in cDMEM (DMEM + 10% FCS, + 2mM  
429 L-glutamine + 100U ml<sup>-1</sup> Penicillin + 100ug ml<sup>-1</sup> streptomycin) for 1 hour at 37°C/5%CO<sub>2</sub>, before  
430 extracellular staining, fixing and permeabilization as detailed. Intracellular Fc receptor blocking followed  
431 by anti-Ki67 staining was then carried out with fluorophore conjugated mAbs in permeabilization buffer. To  
432 assess cytokine production, single cell suspensions were diluted to 5x 10<sup>6</sup> cells ml<sup>-1</sup> in cDMEM and either  
433 stimulated for 4 hrs at 37°C/5% CO<sub>2</sub> with 1 ug ml<sup>-1</sup> PMA/100 ng ml<sup>-1</sup> ionomycin with 1x Brefeldin-A  
434 (GolgiPlug, BD Biosciences) + 1 $\mu$ M Monensin (Sigma) or left unstimulated (golgi -inhibitors alone).  
435 Samples were stained, fixed and permeabilized as described and intracellular staining for Fc receptor  
436 blocking followed by fluorophore conjugated mAbs against IL-5 and IL-13 was carried out in  
437 permeabilization buffer.

438

439 **ILC2 in vitro culture and proliferation analysis with acetylcholine receptor antagonists.** Female  
440 C57BL/6J mice aged 6-8 weeks were infected with *N. brasiliensis* and lungs were processed and ILC2 FACS  
441 sorted at between D5 to D9 p.i. as described. For each experimental run, lungs from 5 mice were pooled and  
442 sorted as a single sample and isolated ILC2 were then split equally between experimental treatment  
443 conditions. Cells were cultured for 72 hours at 37°C / 5% CO<sub>2</sub> in U bottom 96 well plates (Greiner, Cellstar)  
444 in 200  $\mu$ l of cRPMI (RPMI + 10% FCS + 2 mM L-glutamine + 100 U ml<sup>-1</sup> Penicillin + 100 ug ml<sup>-1</sup>  
445 streptomycin) containing 50 ng ml<sup>-1</sup> recombinant human IL-2 (Biolegend) and 50 ng ml<sup>-1</sup> recombinant  
446 murine IL-7 (Biolegend) and either 10  $\mu$ M 1,1-dimethyl-4-diphenylacetoxypiperidinium iodide (4-DAMP)  
447 (Abcam), 10  $\mu$ M mecamlamine hydrochloride (mecamlamine) (Sigma), or an equal volume of drug  
448 vehicle (dH<sub>2</sub>O and DMSO) (vehicle control). Finally, cells were stained as described, including re-staining

449 using the extracellular ILC2 marker panel used to initially sort the cells (to ensure purity of the cultured  
450 population), followed by intranuclear Ki67 staining. Samples were analysed on a BD LSR Fortessa™  
451 analyser.

452  
453  
454 **Endpoint PCR.** Total RNA was extracted by TRIzol/chloroform phase-separation and DNase-1 treatment.  
455 Prior to RNA extraction, mouse brain tissue (used as a for positive control for all acetylcholine receptor  
456 subunit expressions) was homogenised using a TissueLyser II (Qiagen). Reverse transcription (RT) of RNA  
457 was carried out in a 20 µl reaction volume with 50 ng RNA using the Superscript III reverse transcriptase  
458 protocol (Invitrogen) according to the manufacturer's instructions. Polymerase chain reaction (PCR) was  
459 carried out in a 20 µl reaction volume containing: 0.25 pmol forward and reverse primers, 1.25 mM dNTPs,  
460 0.5 U Taq polymerase (New England Biolabs), 1x Thermopol reaction buffer (New England Biolabs), 2 µl  
461 cDNA and dH2O. PCR products were visualised by agarose gel electrophoresis on a gel of appropriate  
462 agarose percentage (1-3%) made with a standard Tris-acetate-EDTA buffer (pH 8.0), utilising GelRed ®  
463 nucleic acid gel stain (Biotium) and a GelDOC-IT TS imaging system (UVP). Primers used for endpoint  
464 PCR are as follows:

465 *Chrm1*: 5'- GGACAACAACACCAGAGGAGA-3'/5'-CGAGGTCACCTTTAGGGTAGGG-3'

466 *Chrm2*: 5'- TGAAAACACGGTTTCCACTTC-3'/5'- GATGGAGGAGGCTTCTTTTTG-3'

467 *Chrm3*: 5'- TTTACATGCCTGTCACCATCA-3'/5'- ACAGCCACCATACTTCCTCCT-3'

468 *Chrm4*: 5'- TGCTCTGTGCATGAACCTTCT-3'/5'- TGGTTATCAGGCACTGTCCCTC-3'

469 *Chrm5*: 5'- CTCTGCTGGCAGTACTTGGTC-3'/5'-GTGAGCCGGTTTTCTCTTCTT-3'

470 *Chrna1*: 5'- GACCATGAAGTCAGACCAGGA-3'/5'- TTAGCTCAGCCTCTGCTCATC-3'

471 *Chrna2*: 5'- TGAGGTCTGAGGATGCTGACT-3'/5'- AGAGATGGCTCCAGTCACAGA-3'

472 *Chrna3*: 5'- GTTGTCCTGTCTGCTCTGTC-3'/5'- CCATCAAGGGTTGCAGAAATA-3'

473 *Chrna4*: 5'- AGATGATGACGACCAACGTGT-3'/5'- ATAGAACAGGTGGGCTTTGGT-3'

474 *Chrna5*: 5'- TGGGCCTTGCAATATCTCAGT-3'/5'- TGACAGTGCCATTGTACCTGA-3'

475 *Chrna7*: 5'- TCAGCAGCTATATCCCAATG-3'/5'- CAGCAAGAATACCAGCAAAGC-3'

476 *Chrb1*: 5'- CTCACTGTGTTCTTGCTGCTG-3'/5'- GAGTTGGTCTCTCTCGGGTTT-3'

477 *Chrb2*: 5'- GGACCATATGCGAAGTGAAGA-3'/5'- ATTTCCAGGGAAAAAGAAGCA-3'

478 *Chrb4*: 5'- TGGCTGCCTGACATAGTTCTC-3'/5'- AGTCCAGGATCCGAACTTCAT-3'

479  
480  
481 **RT-qPCR.** Total lung tissue was homogenised using a Tissuelyser II (Qiagen). FACS purified cells were  
482 lysed directly in TRIzol (Sigma). Total RNA was extracted by TRIzol/chloroform phase-separation, DNase-  
483 I treated, then reverse transcribed using the iScript cDNA synthesis kit (Biorad). RT-qPCR reactions were  
484 carried out using either the PowerUp SYBR Green Mix (ThermoFisher) (*Il13*, *Il5*, *Muc5ac*, *Muc5b*, *Gapdh*,  
485 *Actb*, *Hprt*) or the Quantitect SYBR Green PCR kit (Qiagen) (*Chat*, *18s*) in a ABI 7500 Fast Real-time PCR  
486 thermocycler (Applied Biosystems). RT-qPCR reactions were run in triplicate, with no template and no RT  
487 controls. Relative expression of each gene was calculated by the comparative cycle threshold (Ct) method  
488 ( $2^{-\Delta\Delta CT}$ ) using *Actb*, *Hprt* and *Gapdh* (*Il13*, *Il5*, *Muc5ac*, *Muc5b*) and *18s* (*Chat*) as reference genes. Primer  
489 sequences used for RT-qPCR were as follows:

490 *Chat*; 5'-GGCCATTGTGAAGCGGTTTG-3'/5'-GCCAGGCGGTTGTTTAGATACA-3',

491 *18s*; 5'-TAACGAACGAGACTCTGGCAT-3'/CGGACATCTAAGGGCATCACAG-3'.

492 *Il13*; 5'-TCACTGTAGCCTCCAGGTCTC-3'/5'-TTTCATGGCTGAGGGCTGGTT-3'.

493 *Il5*; 5'-AGCTGGATTTTGGAAAAGAAAAGGG-3'/5'-GCTTTCTGTTGGCATGGGGT-3'.

494 *Muc5ac*; 5'-GACACAAGCCATGCAGAGTCC-3'/5'-CTGGAAAGGCCCAAGCATGT-3'.

495 *Muc5b*; 5'-AGCATCAAAGAGGGTGGTGGG-3'/5'-CTTGCTGTGGGGAGCCTTAAC-3'.

496 *Gapdh*; 5'-GTCATCCCAGAGCTGAACGG-3'/5'-TACTTGGCAGGTTTCTCCAGG-3'.

497 *Actb*; 5'-TTCCTTCTTGGGTATGGAATCCT-3'/5'-TTTACGGATGTCAACGTCACAC-3'.

498 *Hprt*; 5'-ACAGGCCAGACTTTGTTGGA-3'/5'-ACTTGCGCTCATCTTAGGCT-3'

499  
500 **Genotyping.** Genomic DNA (gDNA) was isolated from FACS-purified lung ILC2 from *Rora*<sup>Cre+</sup> *Chat*<sup>LoxP</sup>  
501 and WT mice at day 6 p.i. with *N. brasiliensis* using a DNeasy Blood and Tissue kit (Qiagen). PCR was  
502 performed with gDNA template using Q5 DNA polymerase (NEB) and the primers 5'-  
503 TGAGGGATGATGGATGAATGAG-3'/5'- CTAGGGTTGTTTCCAGAAGGC-3', situated within intronic  
504 regions flanking coding exon 5 of murine *Chat*. Amplified products were separated by agarose gel

505 electrophoresis, and bands corresponding to the WT allele (2076 bp) and the deleted allele (546 bp) were  
506 excised, purified by standard procedures, and sequenced by Eurofins Genomics.

507

508 **Detection of acetylcholine release.** FACS-purified ILC2s were incubated at 37°C for 30 min in 96 well  
509 round-bottomed plates (10<sup>5</sup> cells in 150 µl), centrifuged, supernatants removed, the AChE inhibitor  
510 BW284C51 (Sigma) added at 10 µM and samples stored at -80°C until analysis by HPLC-mass  
511 spectrometry. Control samples were spiked with 50 nM internal standard (acetylcholine -1,1,2,2,-D4  
512 chloride, QMX laboratories).

513

514 **Histology and PAS staining.** Lung or small intestinal tissues were harvested, fixed in 10% buffered  
515 formalin, paraffin embedded and sectioned using standard techniques. Sections were stained with periodic  
516 acid-Schiff's and Haematoxylin and Eosin reagents, photographed at 40x or 100x magnification using a  
517 Zeiss Primo Star microscope and analysed using Image J to determine the Histological Mucus Index (HMI)  
518 by established methods (49). Lung sections were analysed analysed using Image J. Briefly, lung images  
519 were overlaid with a standard grid (2000 Units) and the number of grid units containing PAS positive  
520 epithelial cells were divided by all units containing epithelial cells to establish the Histological Mucus index  
521 (HMI). Intestinal images were analysed with ImageJ and overlaid with a standard grid (1500 Units); 15  
522 crypt-villus segments were selected and the percentage of PAS-positive units per crypt-villus segment were  
523 divided by total units in each crypt-villus to establish HMI.

524

525 **Immunofluorescence.** Jejunal sections were paraffin embedded and sectioned according to standard  
526 techniques. For immunofluorescent staining, tissue slides were incubated at 60°C for 30 min. Next, paraffin  
527 was removed in Neo-clear (Sigma-Aldrich) by washing twice for 5 min. Then, tissue was rehydrated in  
528 decreasing ethanol concentrations (2x 100%, 1x 95%, 1x 80 %, 1x 70 %, (all 3 min) and then in distilled  
529 water. Subsequently, tissue slides were heated and boiled in pH 6 citrate buffer for 15 min using a  
530 microwave. The citrate buffer was cooled to room temperature for 20 min, and slides were washed with  
531 distilled water. Next, tissues sections were marked using a hydrophobic pen (PAP pen, ab2601, Abcam) to

532 prevent leakage. Tissue sections were incubated with blocking buffer (1% BSA, 2% normal goat serum,  
533 0.2% Triton X-100 in PBS) for 1 hour at room temperature in a humidified chamber. Next, slides were  
534 incubated with primary antibody for anti-DCLK1 (Abcam, ab31704) in antibody dilution buffer at 1:250  
535 (0.5% bovine serum albumin, 1% normal goat serum, 0.05% Tween 20 in PBS) at 4°C overnight in a  
536 humidified chamber. The next day, slides were washed 3 times in 0.2% Triton X-100 prepared in PBS for 10  
537 min each. Slides were then incubated with the secondary antibody (1:500, Goat anti-Rabbit IgG Alexa Fluor  
538 488, Invitrogen, A-11034,) and DAPI (1:1000) for 1 hour at room temperature in a dark humidified chamber.  
539 After incubation, slides were washed 3 times with 0.2% Triton X-100 prepared in PBS for 10 min each.  
540 Finally, slides were washed with distilled water and were mounted using Fluoromount G medium  
541 (ThermoFisher Scientific) using cover slips. All the images were acquired with 20x and 40x objectives using  
542 a ZEISS confocal microscope LSM 880 and DCLK1 (green) cells were quantified for  $\geq 30$  crypt-villus pairs  
543 per mouse.

544  
545 **Statistical analysis.** Flow cytometry data was analysed and t-SNE analysis was conducted using FlowJo  
546 software (Treestar). Graphs and statistical tests were carried out using Graphpad prism software (Graphpad).  
547 Normality of data distribution was analysed by Shapiro-Wilk test. Parametric data were analysed by Welch's  
548 t-test, non-parametric data were analysed by Mann-Whitney-U test. Data represent mean  $\pm$  SEM unless  
549 otherwise stated. Statistical significance between groups is indicated as \* $p < 0.05$ , \*\* $p < 0.01$ , \*\*\* $p < 0.001$ ,  
550 \*\*\*\* $p < 0.0001$ , n.s. = non-significant difference ( $p > 0.05$ ).

## 551 H2: Supplementary Materials

553 **Figure S1.** Pulmonary ILC2s acquire a cholinergic phenotype following exposure to *Alternaria*  
554 *alternata*

555 **Figure S2.** Generation of *Rora*<sup>Cre+</sup>*Chat*<sup>LoxP</sup> and validation of *Chat* deletion in lung ILC2s.

556 **Figure S3.** Pulmonary ILC2 cytokine measurements and assessment of numbers and activation  
557 markers of mesenteric lymph node ILC2s in *Chat*<sup>LoxP</sup> and *Rora*<sup>Cre+</sup>*Chat*<sup>LoxP</sup> mice.

**Figure S4. Pulmonary CD4<sup>+</sup> T cell numbers and capacity for Th<sub>2</sub> cytokine expression remains intact in *Rora*<sup>Cre+</sup>*Chat*<sup>loxP</sup> mice**

**References and Notes**

1. K. J. Tracey, The inflammatory reflex. *Nature*. **420**, 853–859 (2002).
2. H. Wang, M. Yu, M. Ochani, C. A. Amella, M. Tanovic, S. Susarla, J. H. Li, H. Wang, H. Yang, L. Ulloa, Y. Al-Abed, C. J. Czura, K. J. Tracey, Nicotinic acetylcholine receptor alpha7 subunit is an essential regulator of inflammation. *Nature*. **421**, 384–388 (2003).
3. Y. N. Tallini, B. Shui, K. S. Greene, K. Y. Deng, R. Doran, P. J. Fisher, W. Zipfel, M. I. Kotlikoff, BAC transgenic mice express enhanced green fluorescent protein in central and peripheral cholinergic neurons. *Physiol. Genomics*. **27**, 391–397 (2006).
4. M. Rosas-Ballina, P. S. Olofsson, M. Ochani, Y. A. L. Sergio I. Valdés- Ferrer, C. Reardon, M. W. Tusche, V. A. Pavlov, U. Andersson, S. Chavan, T. W. Mak, and K. J. Tracey, Kevin, Acetylcholine-Synthesizing T Cells Relay Neural Signals in a Vagus Nerve Circuit Mauricio. *Science (80-. )*. **334**, 98–101 (2015).
5. C. Reardon, G. S. Duncan, A. Brüstle, D. Brenner, M. W. Tusche, P. Olofsson, M. Rosas-Ballina, K. J. Tracey, T. W. Mak, Lymphocyte-derived ACh regulates local innate but not adaptive immunity. *Proc. Natl. Acad. Sci. U. S. A.* **110**, 1410–1415 (2013).
6. M. A. Cox, G. S. Duncan, G. H. Y. Lin, B. E. Steinberg, L. X. Yu, D. Brenner, L. N. Buckler, A. J. Elia, A. C. Wakeham, B. Nieman, C. Dominguez-Brauer, A. R. Elford, K. T. Gill, S. P. Kubli, J. Haight, T. Berger, P. S. Ohashi, K. J. Tracey, P. S. Olofsson, T. W. Mak, Choline acetyltransferase-expressing T cells are required to control chronic viral infection. *Science (80-. )*. **363**, 639–644 (2019).
7. M. Darby, C. Schnoeller, A. Vira, F. Culley, S. Bobat, M. E. Selkirk, W. G. C. Horsnell, The M3 Muscarinic Receptor Is Required for Optimal Adaptive Immunity to Helminth and Bacterial Infection, 1–15 (2015).
8. D. R. Neill, S. H. Wong, A. Bellosi, R. J. Flynn, M. Daly, T. K. a Langford, C. Bucks, C. M. Kane, P. G. Fallon, R. Pannell, H. E. Jolin, A. N. J. McKenzie, Nuocytes represent a new innate effector

- leukocyte that mediates type-2 immunity. *Nature*. **464**, 1367–70 (2010).
9. L. Campbell, M. R. Hepworth, J. Whittingham-Dowd, S. Thompson, A. J. Bancroft, K. S. Hayes, T. N. Shaw, B. F. Dickey, A. L. Flamar, D. Artis, D. A. Schwartz, C. M. Evans, I. S. Roberts, D. J. Thornton, R. K. Grencis, ILC2s mediate systemic innate protection by priming mucus production at distal mucosal sites. *J. Exp. Med.* **216**, 2714–2723 (2019).
10. V. Cardoso, J. Chesné, H. Ribeiro, B. Garcia-Cassani, T. Carvalho, T. Bouchery, K. Shah, N. L. Barbosa-Morais, N. Harris, H. Veiga-Fernandes, Neuronal regulation of type 2 innate lymphoid cells via neuromedin U. *Nature*. **549**, 277–281 (2017).
11. C. S. N. Klose, T. Mahlaköiv, J. B. Moeller, L. C. Rankin, A.-L. Flamar, H. Kabata, L. A. Monticelli, S. Moriyama, G. G. Putzel, N. Rakhilin, X. Shen, E. Kostenis, G. M. König, T. Senda, D. Carpenter, D. L. Farber, D. Artis, The neuropeptide neuromedin U stimulates innate lymphoid cells and type 2 inflammation. *Nature*. **549**, 282–286 (2017).
12. A. Wallrapp, S. J. Riesenfeld, P. R. Burkett, R. E. E. Abdunour, J. Nyman, D. Dionne, M. Hofree, M. S. Cuoco, C. Rodman, D. Farouq, B. J. Haas, T. L. Tickle, J. J. Trombetta, P. Baral, C. S. N. Klose, T. Mahlaköiv, D. Artis, O. Rozenblatt-Rosen, I. M. Chiu, B. D. Levy, M. S. Kowalczyk, A. Regev, V. K. Kuchroo, The neuropeptide NMU amplifies ILC2-driven allergic lung inflammation. *Nature*. **549**, 351–356 (2017).
13. S. Moriyama, J. R. Brestoff, A. L. Flamar, J. B. Moeller, C. S. N. Klose, L. C. Rankin, N. A. Yudanin, L. A. Monticelli, G. G. Putzel, H. R. Rodewald, D. Artis, B2-Adrenergic Receptor-Mediated Negative Regulation of Group 2 Innate Lymphoid Cell Responses. *Science (80-. )*. **359**, 1056–1061 (2018).
14. J. Dalli, R. A. Colas, H. Arnardottir, C. N. Serhan, Vagal Regulation of Group 3 Innate Lymphoid Cells and the Immunoresolvent PCTR1 Controls Infection Resolution. *Immunity*. **46**, 92–105 (2017).
15. H. Veiga-Fernandes, D. Artis, Neuronal-immune system cross-talk in homeostasis. *Science (80-. )*. **359**, 1465–1466 (2018).
16. H. Nagashima, T. Mahlaköiv, H. Y. Shih, F. P. Davis, F. Meylan, Y. Huang, O. J. Harrison, C. Yao, Y. Mikami, J. F. Urban, K. M. Caron, Y. Belkaid, Y. Kanno, D. Artis, J. J. O’Shea,

- 617 Neuropeptide CGRP Limits Group 2 Innate Lymphoid Cell Responses and Constrains Type 2  
618 Inflammation. *Immunity*. **51**, 682-695.e6 (2019).
- 619 17. A. L. Flamar, C. S. N. Klose, J. B. Moeller, T. Mahlaköiv, N. J. Bessman, W. Zhang, S. Moriyama,  
620 V. Stokic-Trtica, L. C. Rankin, G. G. Putzel, H. R. Rodewald, Z. He, L. Chen, S. A. Lira, G.  
621 Karsenty, D. Artis, Interleukin-33 Induces the Enzyme Tryptophan Hydroxylase 1 to Promote  
622 Inflammatory Group 2 Innate Lymphoid Cell-Mediated Immunity. *Immunity*. **52**, 606-619.e6  
623 (2020).
- 624 18. Y. Huang, L. Guo, J. Qiu, X. Chen, J. Hu-Li, U. Siebenlist, P. R. Williamson, J. F. Urban, W. E.  
625 Paul, IL-25-responsive, lineage-negative KLRG1<sup>hi</sup> cells are multipotential “inflammatory” type 2  
626 innate lymphoid cells. *Nat. Immunol.* **16**, 161–169 (2015).
- 627 19. H. J. McSorley, N. F. Blair, K. A. Smith, A. N. J. McKenzie, R. M. Maizels, Blockade of IL-33  
628 release and suppression of type 2 innate lymphoid cell responses by helminth secreted products in  
629 airway allergy. *Mucosal Immunol.* **7**, 1068–78 (2014).
- 630 20. A. S. Mirchandani, A.-G. Besnard, E. Yip, C. Scott, C. C. Bain, V. Cerovic, R. J. Salmond, F. Y.  
631 Liew, Type 2 innate lymphoid cells drive CD4<sup>+</sup> Th2 cell responses. *J. Immunol.* **192**, 2442–8  
632 (2014).
- 633 21. C. J. Oliphant, Y. Y. Hwang, J. A. Walker, M. Salimi, S. H. Wong, J. M. Brewer, A. Englezakis, J.  
634 L. Barlow, E. Hams, S. T. Scanlon, G. S. Ogg, P. G. Fallon, A. N. J. McKenzie, MHCII-mediated  
635 dialog between group 2 innate lymphoid cells and CD4<sup>+</sup> T cells potentiates type 2 immunity and  
636 promotes parasitic helminth expulsion. *Immunity*. **41**, 283–295 (2014).
- 637 22. M. J. Lecomte, C. Bertolus, J. Santamaria, A. L. Bauchet, M. Herbin, F. Saurini, H. Misawa, T.  
638 Maisonobe, P. F. Pradat, M. Nosten-Bertrand, J. Mallet, S. Berrard, Selective disruption of  
639 acetylcholine synthesis in subsets of motor neurons: A new model of late-onset motor neuron  
640 disease. *Neurobiol. Dis.* **65**, 102–111 (2014).
- 641 23. S.-J. Chou, Z. Babot, A. Leingartner, M. Studer, Y. Nakagawa, D. D. M. O’Leary, Geniculocortical  
642 Input Drives Genetic Distinctions Between Primary and Higher-Order Visual Areas. *Science* (80-  
643 ). **340**, 1239–1242 (2013).
- 644 24. Y. Omata, M. Frech, T. Primbs, S. Lucas, D. Andreev, C. Scholtysek, K. Sarter, M. Kindermann,

- 645 N. Yeremenko, D. L. Baeten, N. Andreas, T. Kamradt, A. Bozec, A. Ramming, G. Krönke, S.  
646 Wirtz, G. Schett, M. M. Zaiss, Group 2 Innate Lymphoid Cells Attenuate Inflammatory Arthritis  
647 and Protect from Bone Destruction in Mice. *Cell Rep.* **24**, 169–180 (2018).
- 648 25. J. V. Fahy, B. F. Dickey, Airway Mucus Function and Dysfunction. *N. Engl. J. Med.* **363**, 2233–  
649 2247 (2010).
- 650 26. A. E. Price, H.-E. Liang, B. M. Sullivan, R. L. Reinhardt, C. J. Eisley, D. J. Erle, R. M. Locksley,  
651 Systemically dispersed innate IL-13-expressing cells in type 2 immunity. *Proc. Natl. Acad. Sci.*  
652 **107**, 11489–11494 (2010).
- 653 27. L. Galle-Treger, Y. Suzuki, N. Patel, I. Sankaranarayanan, J. L. Aron, H. Maazi, L. Chen, O.  
654 Akbari, Nicotinic acetylcholine receptor agonist attenuates ILC2-dependent airway hyperreactivity.  
655 *Nat. Commun.* **7**, 1–13 (2016).
- 656 28. B. S. Kim, M. C. Siracusa, S. A. Saenz, M. Noti, L. A. Monticelli, G. F. Sonnenberg, M. R.  
657 Hepworth, A. S. Van Voorhees, M. R. Comeau, D. Artis, TSLP elicits IL-33-independent innate  
658 lymphoid cell responses to promote skin inflammation. *Sci. Transl. Med.* **5**, 170ra16 (2013).
- 659 29. H. Kim, Y. Chang, S. Subramanian, Innate lymphoid cells responding to IL-33 mediate airway-  
660 hyperreactivity independent of adaptive immunity. *J. Allergy ....* **129**, 216–227 (2012).
- 661 30. B. Roediger, R. Kyle, S. S. Tay, A. J. Mitchell, H. A. Bolton, T. V. Guy, S. Y. Tan, E. Forbes-  
662 Blom, P. L. Tong, Y. Köller, E. Shklovskaya, M. Iwashima, K. D. McCoy, G. Le Gros, B. Fazekas  
663 De St Groth, W. Weninger, IL-2 is a critical regulator of group 2 innate lymphoid cell function  
664 during pulmonary inflammation. *J. Allergy Clin. Immunol.* **136**, 1653-1663e7 (2015).
- 665 31. J. C. Nussbaum, S. J. Van Dyken, J. von Moltke, L. E. Cheng, A. Mohapatra, A. B. Molofsky, E. E.  
666 Thornton, M. F. Krummel, A. Chawla, H.-E. Liang, R. M. Locksley, Type 2 innate lymphoid cells  
667 control eosinophil homeostasis. *Nature.* **502**, 245–248 (2013).
- 668 32. J.-E. Turner, P. J. Morrison, C. Wilhelm, M. Wilson, H. Ahlfors, J.-C. Renauld, U. Panzer, H.  
669 Helmbly, B. Stockinger, IL-9-mediated survival of type 2 innate lymphoid cells promotes damage  
670 control in helminth-induced lung inflammation. *J. Exp. Med.* **210**, 2951–65 (2013).
- 671 33. C. S. N. Klose, T. Mahlaköiv, J. B. Moeller, L. C. Rankin, A. L. Flamar, H. Kabata, L. A.  
672 Monticelli, S. Moriyama, G. G. Putzel, N. Rakhilin, X. Shen, E. Kostenis, G. M. König, T. Senda,

- 673 D. Carpenter, D. L. Farber, D. Artis, The neuropeptide neuromedin U stimulates innate lymphoid  
674 cells and type 2 inflammation. *Nature*. **549**, 282–286 (2017).
- 675 34. O. Lockridge, Review of human butyrylcholinesterase structure, function, genetic variants, history  
676 of use in the clinic, and potential therapeutic uses. *Pharmacol. Ther.* **148**, 34–46 (2015).
- 677 35. H. Moriya, Y. Takagi, T. Nakanishi, M. Hayashi, T. Tani, I. Hirotsu, Affinity profiles of various  
678 muscarinic antagonists for cloned human muscarinic acetylcholine receptor (mAChR) subtypes and  
679 mAChRs in rat heart and submandibular gland. *Life Sci.* **64**, 2351–2358 (1999).
- 680 36. F. Dorje, J. Wess, G. Lambrecht, R. Tacke, E. Mutschler, M. R. Brann, Antagonist binding profiles  
681 of five cloned human muscarinic receptor subtypes. *J. Pharmacol. Exp. Ther.* **256**, 727–733 (1991).
- 682 37. R. Gosens, J. Zaagsma, H. Meurs, A. J. Halayko, Muscarinic receptor signaling in the  
683 pathophysiology of asthma and COPD. *Respir. Res.* **7**, 1–15 (2006).
- 684 38. I. S. T. Bos, R. Gosens, A. B. Zuidhof, D. Schaafsma, A. J. Halayko, H. Meurs, J. Zaagsma,  
685 Inhibition of allergen-induced airway remodelling by tiotropium and budesonide: A comparison.  
686 *Eur. Respir. J.* **30**, 653–661 (2007).
- 687 39. B. Bosnjak, C. Tilp, C. Tomsic, G. Dekan, M. P. Pieper, K. J. Erb, M. M. Epstein, Tiotropium  
688 bromide inhibits relapsing allergic asthma in BALB/c mice. *Pulm. Pharmacol. Ther.* **27**, 44–51  
689 (2014).
- 690 40. S. Ohta, N. Oda, T. Yokoe, A. Tanaka, Y. Yamamoto, Y. Watanabe, K. Minoguchi, T. Ohnishi, T.  
691 Hirose, H. Nagase, K. Ohta, M. Adachi, Effect of tiotropium bromide on airway inflammation and  
692 remodelling in a mouse model of asthma. *Clin. Exp. Allergy.* **40**, 1266–1275 (2010).
- 693 41. L. a. Monticelli, D. Artis, Innate lymphoid cells promote lung tissue homeostasis following acute  
694 influenza virus infection. *Nat. Immunol.* **12**, 1045–1054 (2011).
- 695 42. A. B. Molofsky, J. C. Nussbaum, H. E. Liang, S. J. V. Dyken, L. E. Cheng, A. Mohapatra, A.  
696 Chawla, R. M. Locksley, Innate lymphoid type 2 cells sustain visceral adipose tissue eosinophils  
697 and alternatively activated macrophages. *J. Exp. Med.* **210**, 535–549 (2013).
- 698 43. S. H. Wong, J. A. Walker, H. E. Jolin, L. F. Drynan, E. Hams, A. Camelo, J. L. Barlow, D. R.  
699 Neill, V. Panova, U. Koch, F. Radtke, C. S. Hardman, Y. Y. Hwang, P. G. Fallon, A. N. J.  
700 McKenzie, Transcription factor ROR $\alpha$  is critical for nuocyte development. *Nat. Immunol.* **13**, 229–

701 36 (2012).

- 702 44. T. Y. F. Halim, A. MacLaren, M. T. Romanish, M. J. Gold, K. M. McNagny, F. Takei, Retinoic-  
703 Acid-Receptor-Related Orphan Nuclear Receptor Alpha Is Required for Natural Helper Cell  
704 Development and Allergic Inflammation. *Immunity*. **37**, 463–474 (2012).
- 705 45. D. N. Cook, H. S. Kang, A. M. Jetten, Retinoic Acid-Related Orphan Receptors (RORs):  
706 Regulatory Functions in Immunity, Development, Circadian Rhythm, and Metabolism. *Nucl.*  
707 *Recept. Res.* **2**, 139–148 (2015).
- 708 46. R. M. Maizels, H. H. Smits, H. J. McSorley, Modulation of Host Immunity by Helminths: The  
709 Expanding Repertoire of Parasite Effector Molecules. *Immunity*. **49**, 801–818 (2018).
- 710 47. M. E. Selkirk, O. Lazari, J. B. Matthews, *Functional genomics of nematode acetylcholinesterases*.  
711 (2005), vol. 131 Suppl.
- 712 48. M. Camberis, G. Le Gros, J. Urban, in *Current Protocols in Immunology* (John Wiley & Sons, Inc.,  
713 Hoboken, NJ, USA, 2003; <http://doi.wiley.com/10.1002/0471142735.im1912s55>), vol. Chapter 19,  
714 p. Unit 19.12.
- 715 49. W. G. C. Horsnell, M. G. Darby, J. C. Hoving, N. Nieuwenhuizen, H. J. McSorley, H. Ndlovu, S.  
716 Bobat, M. Kimberg, F. Kirstein, A. J. Cutler, B. DeWals, A. F. Cunningham, F. Brombacher, IL-  
717 4R $\alpha$ -Associated Antigen Processing by B Cells Promotes Immunity in *Nippostrongylus brasiliensis*  
718 Infection. *PLoS Pathog.* **9**, 1–12 (2013).

719 **Acknowledgments**

720 **General:** We thank Mark Bennett for mass spectrometric determination of ACh, Henry McSorley for the  
721 kind gift of *Alternaria alternata* extract, and Jane Srivistava and Catherine Simpson for technical assistance  
722 with flow cytometry-assisted cell sorting.  
723

724 **Funding:** We thank the Wellcome Trust and the BBSRC for supporting this work through a PhD studentship  
725 to LBR (097011) and a project grant to MES and DW (BB/R015856/1). RV was supported by a Medical  
726 Research Council PhD studentship (MR/J500379/1), and RB was initially supported by a scholarship from  
727 the Association Philippe Jabre (apj.org.ib). Royal Society International Exchange grant: IES\R1\180108,  
728  
729  
730

731 LeStudium-Marie Cure Fellowship supported work by JP, DS, CM, BR, VQ and WGCH. NRF Competitive  
732 Support for Rated Researchers grant: 111815 supported work by MD, JP and WGCH. MJO and NP were  
733 supported by the Norwegian Research Council (Centre of Excellence grant 223255/F50, and 'Young  
734 Research Talent' 274760 to MJO).

735

736 **Author contributions:** Conception and design: LBR MES CS WGCH BR VQ KG DRW. Experimental  
737 work: LBR CS RB MD JP MJO NP CM DS SB RV WGCH MES. Analysis and interpretation: LBR CS  
738 MD JP MJO NP WGCH MES. Drafting the manuscript: LBR WGCH MES.

739

740 **Competing interests:** The authors declared no competing interests.

741

742 **Data and materials availability:** If data are in an archive, include the accession number or a placeholder  
743 for it. Also include any materials that must be obtained through an MTA.

744

745

746

## 747 **Figure Legends**

748

749 **Figure 1. Pulmonary ILC2s acquire a cholinergic phenotype associated with an enhanced activation**  
750 **state during infection with *Nippostrongylus brasiliensis*.** **A)** Proportion and total number of CD45<sup>+</sup>  
751 leucocytes expressing ChAT-eGFP in the lungs of naïve ChAT<sup>BAC</sup>-eGFP mice or animals infected with *N.*  
752 *brasiliensis* (*Nb*) at day (D) 2,4,7, and 21 post infection (p.i.). **B)** Proportion of parental leucocyte populations  
753 expressing ChAT-eGFP in the lungs of naïve ChAT<sup>BAC</sup>-eGFP mice or animals infected with *Nb* at D4 p.i..  
754 **C)** Representative flow cytometry plots of ChAT-eGFP expression by ILC2s (CD45<sup>+</sup>CD90<sup>+</sup>Lineage-  
755 CD127<sup>+</sup>ICOS<sup>+</sup>ST2<sup>+</sup>) in wild type C57BL/6J mice infected with *Nb* (eGFP gating control), naïve ChAT<sup>BAC</sup>-  
756 eGFP animals or infected ChAT<sup>BAC</sup>-eGFP animals at D7 p.i. **D)** Dynamics of ChAT expression by ILC2s in  
757 the lungs and BAL throughout infection with *Nb*. **E)** Expression of *Chat* transcripts assayed by RT-qPCR in  
758 FACS-sorted eGFP<sup>+</sup> and eGFP<sup>-</sup> pulmonary ILC2s from *Nb*-infected ChAT<sup>BAC</sup>-eGFP animals, normalised to  
759 18s rRNA expression and relative to expression from ILC2s from naïve controls. **F)** Quantification of basal  
760 acetylcholine (ACh) release from FACS-sorted pulmonary ILC2s from C57BL6/J naïve and *Nb*-infected  
761 animals. **G)** Mean fluorescence intensity (MFI) of ST2 expressed by ChAT-eGFP negative and ChAT-  
762 eGFP<sup>+</sup> ILC2s in the lungs throughout infection with *Nb*. **H)** Geometric MFI (gMFI) of ICOS expressed by

763 ChAT-eGFP<sup>-</sup> and ChAT-eGFP<sup>+</sup> ILC2s in the lungs throughout infection with *Nb*. Joined data points in (H-  
764 G) represent ChAT<sup>+</sup> and ChAT<sup>-</sup> ILC2 from individual mice. n = 4 to 5 mice/group. Data are representative  
765 of N =3 and graphs present mean ± SEM. \*p<0.05, \*\*p<0.01, \*\*\*p< 0.001, \*\*\*\*p<0.0001, n.s. = non-  
766 significant (p>0.05).

767

**Figure 2. ChAT-eGFP<sup>+</sup> ILC2s display a range of phenotypes which support positive association of  
ChAT expression by ILC2s with cellular activation state.** **A)** Identification of population clusters (left)  
representing natural ILC2 (nILC2: IL17RB<sup>-</sup>ST2<sup>+</sup>Klrg1<sup>+</sup>CD90<sup>hi</sup>), inflammatory ILC2 (iILC2:  
IL17RB<sup>+</sup>ST2<sup>lo</sup>Klrg1<sup>+</sup>CD90<sup>lo</sup>) and nILC2/iILC2 with an activated-like phenotypic profile (nILC2a: IL17RB<sup>-</sup>  
ST2<sup>+</sup>Klrg1<sup>+</sup>CD90<sup>+</sup>, iILC2a: IL17RB<sup>+</sup>ST2<sup>+</sup>Klrg1<sup>+</sup>CD90<sup>+</sup>) within the lungs of *N. brasiliensis* (*Nb*)-infected  
ChAT-eGFP<sup>BAC</sup> mice at day 7 post infection (D7 p.i.). Clustering analysis was conducted using t-distributed  
stochastic neighbour embedding (t-SNE), with the parameter of ChAT-eGFP expression omitted, carried  
out on total lung ILC2s (identified as live, single cells, CD45<sup>+</sup>Lineage<sup>neg</sup>CD127<sup>+</sup>ICOS<sup>+</sup>CD90<sup>+</sup> and  
expressing either or both ST2 and/or IL-17RB) with indicated populations identified on the basis of various  
phenotypic markers and marker expression levels as indicated by the heatmap plots shown (right). **B)**  
Heatmap plot showing locations of greatest ChAT-eGFP expression amongst ILC2 clusters as defined  
through t-SNE in (A). **C)** Clustering analysis carried out by t-distributed stochastic neighbour embedding (t-  
SNE) as in (A) but with the parameter of ChAT-eGFP expression included (left) and heatmap plot of ChAT-  
eGFP expression to identify ChAT<sup>+</sup> cell clusters, designated C1, C2 and C3 (right). **D)** Representative  
histogram overlays of indicated marker expression for the indicated populations identified within a given  
biological samples. **E)** Contributions of populations C1, C2, C3 to total ChAT-eGFP<sup>+</sup> ILC2 present in the  
lungs of ChAT-eGFP<sup>BAC</sup> mice at D7 p.i, expressed as the contributing proportion of each population to the  
total. **F)** Representative histogram overlays for the indicated marker expressions of total ChAT-eGFP<sup>+</sup> and  
ChAT-eGFP<sup>neg</sup> ILC2s (identified as live, single cells, CD45<sup>+</sup>Lineage<sup>neg</sup>CD127<sup>+</sup>ICOS<sup>+</sup>CD90<sup>+</sup> and expressing  
either or both ST2 and/or IL-17RB) present in the lungs of naïve and infected ChAT-eGFP<sup>BAC</sup> mice at D7  
p.i.. **G)** Mean fluorescence intensity (MFI) of ST2 expressed by total ILC2 and ChAT-eGFP negative and  
ChAT-eGFP<sup>+</sup> ILC2s in the lungs of naïve and infected mice as in (F). **H)** As for (G) but for ICOS geometric  
MFI (gMFI). Data shown is representative of observations and population comparisons made in n = 3 male

791 ChAT-eGFP<sup>BAC</sup> mice in both naïve and infected treatment groups. N=1. Data shown as mean ± SEM and  
792 analysed by Shapiro-Wilk normality testing followed by Welch's t-test , \*p<0.05, \*\*p<0.01. n.s. = non-  
793 significant (p>0.05).

794

795 **Figure 3. Mesenteric lymph node ILC2s upregulate expression of ChAT following infection with**  
796 ***Nippostrongylus brasiliensis*. A)** Representative flow cytometry gating indicating identification of total  
797 ILC2s and ChAT-eGFP<sup>+</sup> and ChAT-eGFP<sup>neg</sup> ILC2s from the mesenteric lymph nodes (MLNs) of naïve and  
798 infected ChAT-eGFP<sup>BAC</sup> mice at D7 p.i. *N. brasiliensis* -infected C57BL/6J control sampled included to  
799 indicate ChAT-eGFP<sup>+</sup> gating control. **B)** Quantification of ChAT-eGFP<sup>+</sup> ILC2s from naïve and D7 p.i.  
800 ChAT-eGFP<sup>BAC</sup> mice expressed as a proportion of total ILC2s as shown in (A). **C)** Quantification of the  
801 number of total, ChAT-eGFP<sup>+</sup> and ChAT-eGFP<sup>neg</sup> ILC2s from MLNs of naïve and D7 p.i. ChAT-eGFP<sup>BAC</sup>  
802 mice. **D)** Representative histogram overlays for the indicated marker expressions of total ChAT-eGFP<sup>+</sup> and  
803 ChAT-eGFP<sup>neg</sup> MLN ILC2s of naïve and infected ChAT-eGFP<sup>BAC</sup> mice at D7 p.i.. **E)** Mean fluorescence  
804 intensity (MFI) of ST2 expressed by total ILC2 and ChAT-eGFP negative and ChAT-eGFP<sup>+</sup> ILC2s in the  
805 MLNs of naïve and infected mice as in (D). **F)** As for (E) but for ICOS geometric MFI (gMFI). **G)**  
806 Representative flow cytometry plot of ChAT-eGFP expression by small intestinal lamina propria (siLP)  
807 ILC2s in naïve ChAT<sup>BAC</sup>-eGFP animals. Gate number represents proportion of ILC2 parental gate. Data  
808 shown is representative of observations and population comparisons made in n = 3 male ChAT-eGFP<sup>BAC</sup>  
809 mice in both naïve and infected treatment groups (N = 1), apart from data shown in (G) which is  
810 representative of results in n = 2 mice. Data shown as mean ± SEM and analysed by Shapiro-Wilk normality  
811 testing followed by Welch's t-test , \*p<0.05, \*p<0.01, \*\*\*p<0.001, \*\*\*\*p<0.0001.

812

813 **Figure 4. The cholinergic phenotype of pulmonary ILC2s is induced by IL-25 and IL-33 and is**  
814 **augmented by IL-2. A)** Proportion of pulmonary ILC2s expressing ChAT-eGFP following sorting by FACS  
815 and 24 hr culture with medium only (control), IL-33 or IL-7. **B)** Proportion of ILC2s in the lungs of  
816 ChAT<sup>BAC</sup>-eGFP mice, 24 hrs following intranasal dosing with PBS, IL-33, IL-25, or thymic stromal  
817 lymphopoietin (TSLP). **C)** As for (B) but for mean fluorescence intensity (MFI) of eGFP expressed by  
818 ILC2s. **D)** As for (A) but for the parental leucocyte populations indicated. **E)** Representative flow cytometry

819 plot of IL-17RB expression by lung ILC2s in naïve ChAT<sup>BAC</sup>-eGFP animals. Gate number represents  
820 proportion of ILC2 (CD45<sup>+</sup>CD90<sup>+</sup>Lineage<sup>-</sup>CD127<sup>+</sup>ICOS<sup>+</sup> then ST2<sup>+</sup> and/or IL-17RB<sup>+</sup> live single cells). **F)**  
821 Quantification of IL-17RB<sup>+</sup> lung ILC2s as in (E). **G)** Proportion of ChAT-eGFP<sup>+</sup> ILC2s following *in vitro*  
822 culture of FACS purified total lung CD45<sup>+</sup> cells for 24 hrs with the indicated combinations of IL-33, IL-25  
823 and IL-2. **H)** As for (G) but for eGFP MFI of ILC2s. n = 3-5 animals per group. Data (A-D) and (G-H) are  
824 representative of N = 2. Data (E-F) are representative of n = 3 mice per treatment group, N=1. Graphs present  
825 mean  $\pm$  SEM. Analysis carried out by Shapiro-Wilk test followed by Welch's t-test. \*p<0.05, \*\*p<0.01,  
826 \*\*\*p< 0.001, n.s. = non-significant (p>0.05).

827

828 **Figure 5. RoRa-driven disruption of ChAT expression impairs pulmonary type 2 immunity and**  
829 **expulsion of *Nippostrongylus brasiliensis* from the gut. A)** Recovery of adult worms from the lungs and  
830 intestines of *Chat*<sup>LoxP</sup> and *Rora*<sup>Cre+</sup>*Chat*<sup>LoxP</sup> mice at Day 2 (D2) and D6 post infection (p.i.) respectively, with  
831 *N. brasiliensis* (*Nb*) ( N = 2-3) . **B)** Total number of eosinophils in the lungs of *Nb*-infected *Chat*<sup>LoxP</sup> and  
832 *Rora*<sup>Cre+</sup>*Chat*<sup>LoxP</sup> mice at D6 p.i (N = 1). **C)** RT-qPCR analysis of *Il13* (left) and *Il5* (right) transcript  
833 expression in lung tissue of *Nb*-infected *Rora*<sup>Cre+</sup>*Chat*<sup>LoxP</sup> mice, represented as fold change against expression  
834 in infected *Chat*<sup>LoxP</sup> lung samples. Each data point represents results from 1 animal. **D)** as for (C) but for  
835 analysis of *Muc5ac* and *Muc5b* expression. **E)** Representative lung sections from D6 *Nb*-infected *Chat*<sup>LoxP</sup>  
836 and *Rora*<sup>Cre+</sup>*Chat*<sup>LoxP</sup> mice (2 per genotype) showing Periodic Acid-Schiff<sup>+</sup> (PAS) and Hematoxylin and  
837 Eosin (H&E) staining (scale bar: 100 $\mu$ m). **F)** Quantification of PAS stained lung sections (n = 5 mice per  
838 group, data representative of N = 2). Data show mean  $\pm$  SEM and analysed by Mann-Whitney U test,  
839 \*p<0.05, \*\*p<0.01, n.s. = non-significant (p>0.05).

840

841 **Figure 6. Impaired immunity to *Nippostrongylus brasiliensis* in *Rora*<sup>Cre+</sup>*Chat*<sup>LoxP</sup> mice is associated with**  
842 **defective intestinal epithelial effector responses. A)** Representative intestinal sections from *N. brasiliensis*  
843 (*Nb*)-infected *Chat*<sup>LoxP</sup> and *Rora*<sup>Cre+</sup>*Chat*<sup>LoxP</sup> mice at D7 p.i. (2 per genotype) showing Periodic Acid-Schiff<sup>+</sup>  
844 (PAS) staining (scale bar: 50  $\mu$ m) at 40x and 100x magnification. **B)** Quantification of PAS stained sections  
845 from (A). **C)** Representative immunofluorescence staining for doublecortin-like kinase 1 (*Dclk1*) expressing  
846 Tuft cells (green) with DAPI counterstain (blue) in jejunal sections of *Nb*-infected *Chat*<sup>LoxP</sup> and

847 *Rora*<sup>Cre+</sup>*Chat*<sup>LoxP</sup> mice at D7 p.i. at 20x magnification (scale bar: 50  $\mu$ m). **D**) Quantification of Dclk1<sup>+</sup> Tuft  
848 cells in crypt (left), villus (center) and crypt+villus (right) regions of sections as in (C). **E**) Quantification of  
849 Dclk1<sup>+</sup> Tuft cells as in (H), expressed as the ratio of cells in villus/ crypt regions per biological replicate  
850 sample. Data represent n= 5-6 mice per experimental group, N = 2. Data shown as mean  $\pm$  SEM and analysed  
851 by Mann-Whitney U test, \*p<0.05, \*\*p<0.01, \*\*\*p<0.001, n.s. = non-significant (p>0.05).

852

853 **Figure 7. RoRa-driven disruption of ChAT expression in ILC2 limits ILC2 proliferation.** **A**) Number  
854 of ILC2s in the lungs of naïve and *N. brasiliensis* (*Nb*)-infected *Chat*<sup>LoxP</sup> and *Rora*<sup>Cre+</sup>*Chat*<sup>LoxP</sup> mice at D6  
855 p.i. **B**) Total number of IL-13<sup>+</sup> (left), IL-5<sup>+</sup> (centre) and IL-13<sup>+</sup>IL-5<sup>+</sup> ILC2s (right) in the lungs of naïve and  
856 *Nb*-infected (D6 p.i.) *Chat*<sup>LoxP</sup> and *Rora*<sup>Cre+</sup>*Chat*<sup>LoxP</sup> mice. **C**) Representative flow cytometry plots of Ki67  
857 staining in lung ILC2s from naïve and *Nb*-infected *Chat*<sup>LoxP</sup> and *Rora*<sup>Cre+</sup>*Chat*<sup>LoxP</sup> mice at D6 p.i. Gate  
858 numbers represent proportion of ILC2 parental gate. Positive gate set with fluorescence-minus-one control  
859 for Ki67. **D**) Summary data for proportion of Ki67<sup>+</sup> lung ILC2s from naïve and infected *Chat*<sup>LoxP</sup> and  
860 *Rora*<sup>Cre+</sup>*Chat*<sup>LoxP</sup> mice. **E**) as for (D) but for total number of Ki67<sup>+</sup> ILC2. **F**) Representative histogram  
861 overlays for ICOS expression by lung ILC2s from naïve and *Nb*-infected *Chat*<sup>LoxP</sup> and *Rora*<sup>Cre+</sup>*Chat*<sup>LoxP</sup> mice  
862 at D6.p.i. As all ILC2s are ICOS<sup>+</sup>, ICOS<sup>neg</sup> ILCs (CD45<sup>+</sup>CD90<sup>+</sup>Lineage<sup>+</sup>CD127<sup>+</sup>ICOS<sup>neg</sup>) from *Nb*-infected  
863 *Chat*<sup>LoxP</sup> mice are also shown as a biological negative control for ICOS expression. **G**) Summary data for  
864 ICOS mean fluorescence intensity (MFI) of lung ILC2s from naïve and infected *Chat*<sup>LoxP</sup> and  
865 *Rora*<sup>Cre+</sup>*Chat*<sup>LoxP</sup> mice. **H**) Muscarinic acetylcholine receptor (mAChR) subtype expression analysis (*Chrm1*-  
866 5) conducted on cDNA from FACS sorted ChAT-eGFP<sup>+</sup> and ChAT-eGFP<sup>neg</sup> lung ILC2s of *Nb*-infected  
867 ChAT-eGFP<sup>BAC</sup> mice, by endpoint PCR analysis, visualized by agarose gel electrophoresis. C57BL/6J brain  
868 tissue cDNA from was prepared and used as a positive control for AChR gene expressions. **I**) As for (H) but  
869 for analysis of nicotinic acetylcholine receptor (nAChR) alpha subunits (*Chrna1-5,7*) and beta subunits  
870 (*Chrnb1-4*) expressions. **J**) Representative flow cytometry plots and summary data (**K**) for Ki67 expression  
871 (represented as % of ILC2 parent) by FACS sorted C57BL/6J female lung ILC2s from *N. brasiliensis* -  
872 infected mice, cultured for 72 hours *in vitro* with recombinant IL-7 and IL-2 only (50 ng ml<sup>-1</sup>) or in the  
873 presence of 10  $\mu$ M of the muscarinic receptor antagonist 1,1-dimethyl-4-diphenylacetoxypiperidinium  
874 iodide (4-DAMP) or the nicotinic receptor antagonist mecamylamine hydrochloride (mecamylamine), or

875 with an equivalent volume of reagent vehicles (dH2O, DMSO) added to the culture medium (vehicle). L)  
876 Data from (K) expressed as vehicle control normalized values for each independent experimental run. Data  
877 A-G n=5 mice/ group, N =2. Data H-I is representative of cells pooled from n=6 *Nb*-infected ChAT-eGFP<sup>BAC</sup>  
878 mice, sorted as ChAT-eGFP<sup>+</sup> and ChAT-eGFP<sup>neg</sup> lung ILC2s at D11 p.i, N = 1. Data J-L, is representative  
879 of N = 4 with similar results ( raw data shown in (K), using cells pooled from n=5 mice per experiment. Data  
880 show mean  $\pm$  SEM and analysed by Mann-Whitney U test, \* $p < 0.05$ , \*\* $p < 0.01$ , \*\*\* $p < 0.001$ , \*\*\*\* $p < 0.0001$ ,  
881 n.s. = non-significant ( $p > 0.05$ ).

882

883

884

885

886

887

888

889

890

891

892

893

894

895

Supplementary Materials

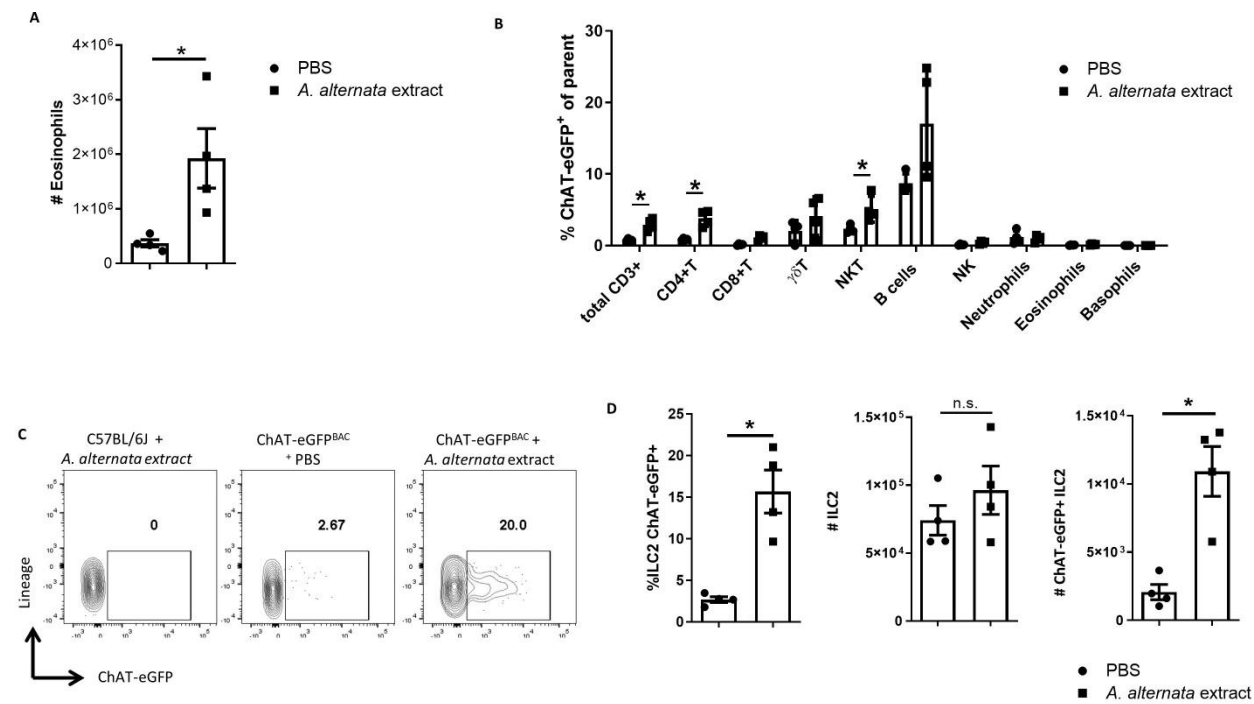
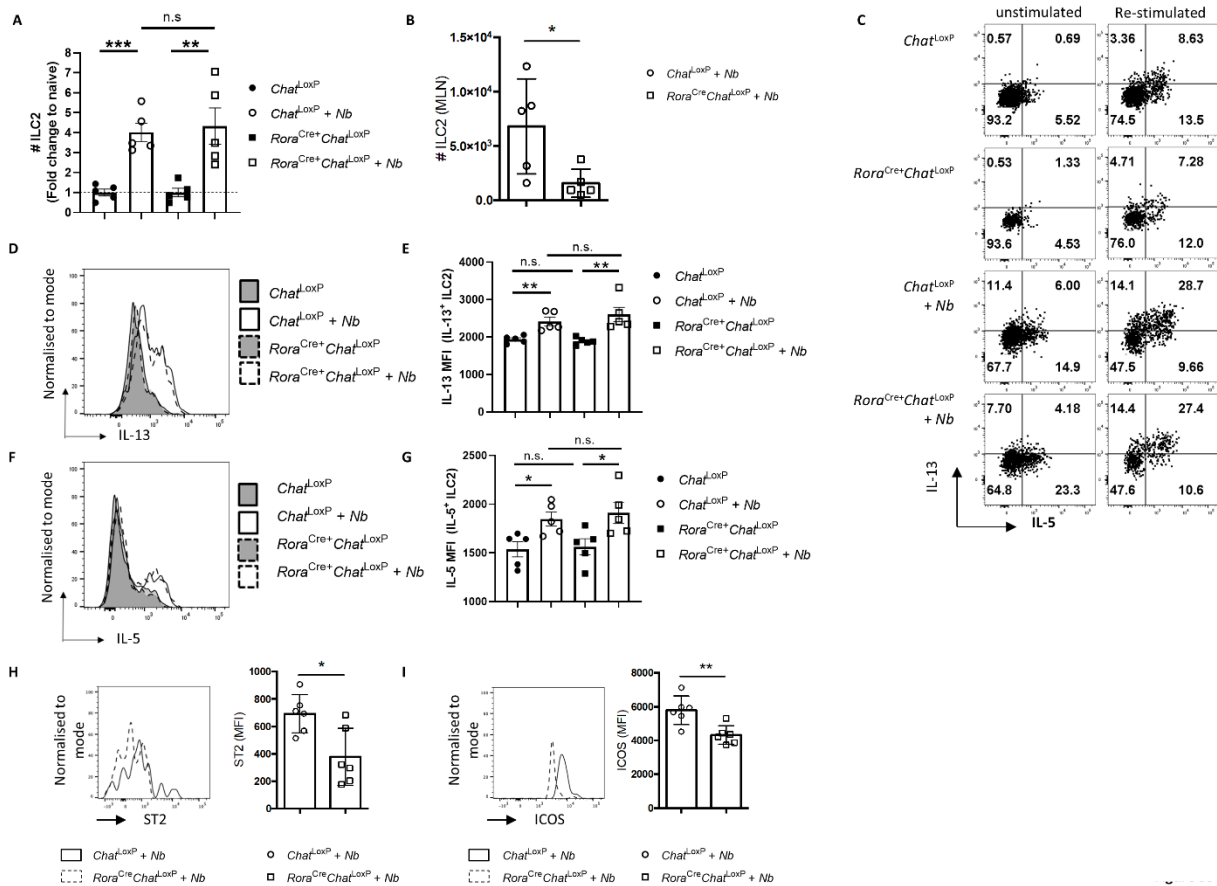


**Figure S1. Pulmonary ILC2s acquire a cholinergic phenotype following exposure to *Alternaria alternata*.** **A)** Intranasal administration of *Alternaria alternata* extract stimulates pulmonary eosinophilia. **B)** Proportion of parental cell populations expressing ChAT-eGFP in the lungs of ChAT<sup>BAC</sup>-eGFP mice 24 hrs following intranasal dosing with PBS (vehicle control) or *A. alternata* extract. **C)** Representative flow cytometry plots of ChAT-eGFP expression by ILC2s in lungs of wild type C57BL/6J mice exposed to *A. alternata* extract (eGFP gating control), or ChAT<sup>BAC</sup>-eGFP mice dosed with PBS or *A. alternata* allergenic extract. **D)** ILC2 responses in the lungs of ChAT<sup>BAC</sup>-eGFP mice 24 hrs following intranasal dosing with PBS or *A. alternata* extract including (from left to right): proportion (%) of ChAT-eGFP+ ILC2s, total number (#) of ILC2s in the lung, and total number of ChAT-eGFP+ ILC2s. n = 4 to 5 mice/group. Data are representative of N=2 and represent mean ± SEM. \*p<0.05, n.s. = non-significant (p>0.05).



959  
960  
961  
962  
963  
964  
965  
966  
967  
968  
969



970 **Figure S3. Pulmonary ILC2 cytokine measurements and assessment of numbers and activation**  
 971 **markers of mesenteric lymph node ILC2s in *Chat<sup>LoxP</sup>* and *Rora<sup>Cre+</sup>Chat<sup>LoxP</sup>* mice.** **A)** Number of ILC2s  
 972 in naïve and *N. brasiliensis* (*Nb*)-infected *Rora<sup>Cre+</sup>Chat<sup>LoxP</sup>* and *Chat<sup>LoxP</sup>* mice expressed as the fold change  
 973 from the average number of ILC2s in naïve mice of each genotype (normalized to a value of 1). **B)** Number  
 974 of ILC2s from mesenteric lymph nodes (MLN) of *Rora<sup>Cre+</sup>Chat<sup>LoxP</sup>* and *Chat<sup>LoxP</sup>* mice infected with *Nb*. **C)**  
 975 Representative flow cytometry plots for intracellular staining of lung ILC2 for IL-13 and IL-5 in  
 976 unstimulated (Monensin only) and re-stimulated (PMA/Ionomycin+ Monensin) culture conditions.  
 977 Quadrants were set using fluorescence minus one controls for IL-13 and IL-5. Quadrant numbers represent  
 978 the proportion of the ILC2 parental population. **D)** Representative histogram overlays of IL-13 intracellular  
 979 staining of lung ILC2 from re-stimulated lung samples and **(E)** summary of IL-13 mean fluorescence  
 980 intensity (MFI) analysis of those samples. **F)** and **(G)** as for **(D)** and **(E)** respectively, but for intracellular  
 981 staining of IL-5. **H)** Representative histogram overlays for ST2 expression by MLN ILC2s from infected  
 982 *Chat<sup>LoxP</sup>* and *Rora<sup>Cre+</sup>Chat<sup>LoxP</sup>* mice (left) and summary data for ST2 mean fluorescence intensity (MFI) of  
 983 MLN ILC2s (right). **I)** As for **(H)** but for ICOS expression by MLN ILC2s. Timepoints of infection were



1007  
1008  
1009  
1010  
1011  
1012  
1013  
1014  
1015  
1016  
1017  
1018  
1019  
1020  
1021  
1022  
1023  
1024  
1025  
1026  
1027  
1028  
1029  
1030

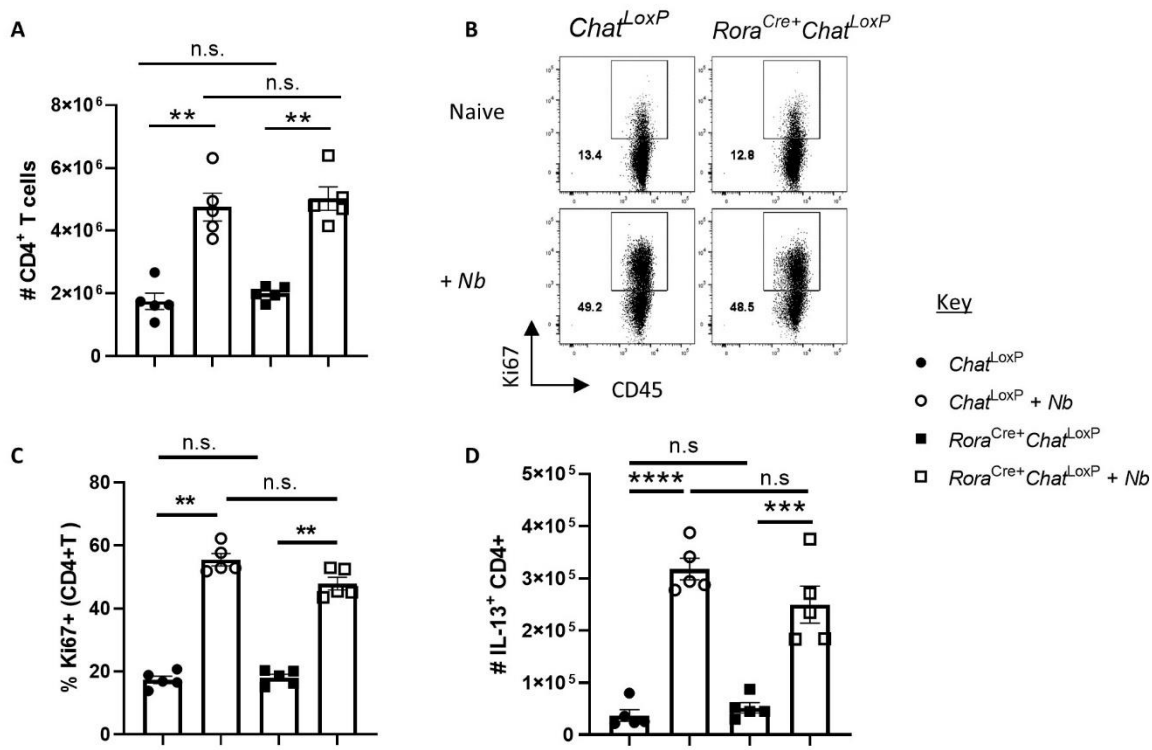


**Figure S4. Pulmonary CD4<sup>+</sup> T cell numbers and capacity for Th<sub>2</sub> cytokine expression remains intact in *Rora*<sup>Cre+</sup> *Chat*<sup>loxP</sup> mice.** **A)** Total number of CD4<sup>+</sup> T cells in the lungs of naïve and infected *Chat*<sup>LoxP</sup> and *Rora*<sup>Cre+</sup> *Chat*<sup>LoxP</sup> mice. **B)** Representative flow cytometry plots of Ki67 staining in lung CD4<sup>+</sup> T cells from naïve and infected *Chat*<sup>LoxP</sup> and *Rora*<sup>Cre+</sup> *Chat*<sup>LoxP</sup> mice. Gate numbers represent proportion of ILC2 parental gate. Positive gate set with fluorescence minus one control for Ki67. **C)** Proportion of lung CD4<sup>+</sup> T cells from naïve and *N. brasiliensis* (*Nb*)-infected *Chat*<sup>LoxP</sup> and *Rora*<sup>Cre+</sup> *Chat*<sup>LoxP</sup> mice expressing Ki67. **D)** Number of IL-13<sup>+</sup> CD4<sup>+</sup> T cells in the lungs of naïve and infected *Chat*<sup>LoxP</sup> and *Rora*<sup>Cre+</sup> *Chat*<sup>LoxP</sup> mice. n = 5 mice per group, N = 2. Timepoints of infection were D6 p.i. Data represent mean ± SEM and analysed by Mann Whitney U test. \*p<0.05, \*\*p<0.01, n.s. = non-significant (p>0.05).